

Electronic Thesis and Dissertation Repository

---

8-6-2014 12:00 AM

# The Development of a Digital X-ray Imaging System for The Characterization of Transmission of Whole-Body Vibration in Mice

Zhengyi Hu  
*The University of Western Ontario*

Supervisor  
David W. Holdsworth  
*The University of Western Ontario*

Graduate Program in Medical Biophysics  
A thesis submitted in partial fulfillment of the requirements for the degree in Master of Science  
© Zhengyi Hu 2014

Follow this and additional works at: <https://ir.lib.uwo.ca/etd>



Part of the [Medical Biophysics Commons](#)

---

## Recommended Citation

Hu, Zhengyi, "The Development of a Digital X-ray Imaging System for The Characterization of Transmission of Whole-Body Vibration in Mice" (2014). *Electronic Thesis and Dissertation Repository*. 2409.

<https://ir.lib.uwo.ca/etd/2409>

This Dissertation/Thesis is brought to you for free and open access by Scholarship@Western. It has been accepted for inclusion in Electronic Thesis and Dissertation Repository by an authorized administrator of Scholarship@Western. For more information, please contact [wlsadmin@uwo.ca](mailto:wlsadmin@uwo.ca).

THE DEVELOPMENT OF A DIGITAL X-RAY IMAGING SYSTEM FOR THE  
CHARACTERIZATION OF TRANSMISSION OF WHOLE-BODY VIBRATION IN  
MICE

by

Zhengyi Hu

Graduate Program in Medical Biophysics

A thesis submitted in partial fulfillment  
of the requirements for the degree of  
Master of Science

The School of Graduate and Postdoctoral Studies  
The University of Western Ontario  
London, Ontario, Canada

© Zhengyi Hu 2014

## Abstract

Mechanical stimulus such as whole-body vibration (WBV) has shown to promote bone formation both in humans and animals. WBV has been hypothesized as a potentially useful osteoporosis intervention. While the transmission of WBV has been well characterized in humans, there is currently a lack of knowledge in the transmission of vibration in small animal models, such as mice, due to the lack of an implantable accelerometer appropriate to make such measurements. This thesis introduces an image-based method to quantify transmission of vibration in mice using x-ray imaging. Specifically, it utilizes motion blur of fiducial markers, which are implanted into the mouse tibia and femur. Vibration characteristics *in vivo* were characterized over the range of 15-40 Hz. Resonance was observed in the femur at 25 Hz and reduction in transmission in the tibia at 30 Hz. These findings provide an estimate of the magnitude of vibration transmitted into the animal's limb.

## Keywords

Whole-body vibration, Osteoporosis, Mice, Bone Resonance, Skeletal Loading, Tungsten Carbide Implant

## Co-Authorship Statement

Chapter 2 was co-authored by Dr. Ian Welch, Dr. Xunhua Yuan, Steven Pollmann, Hristo Nikolov, and Dr. David Holdsworth. Dr. Welch assisted in the implantation of the fiducial marker in mice. Dr. Yuan assisted in data collection. Steven wrote the code for image unwrap algorithm. Hristo designed and built the vibration platform. Dr. Holdsworth assisted in conception of the idea, experimental design, and data analysis. All of the authors critically reviewed the manuscript. I was involved in the design and construction of mouse restrainer, imaging system, conducted experiments, wrote code for MATLAB, performed the data analysis, and wrote the manuscript.

Chapter 3 was co-authored by Dr. Ian Welch, Dr. Xunhua Yuan, Dr. S. Jeffrey Dixon, and Dr. David Holdsworth. Dr. Welch assisted in the implantation of the fiducial marker in mice. Dr. Yuan assisted in data collection. Dr. Dixon and Dr. Holdsworth assisted in conception of the idea, experimental design, and data analysis. All of the authors critically reviewed the manuscript. I was involved in the design and construction of mouse restrainer, imaging system, conducted experiments, wrote code for MATLAB, performed the data analysis, and wrote the manuscript.



## Acknowledgments

First of all, I would like to thank my supervisor Dr. David Holdsworth for his guidance and support throughout my Master at the Robarts Research Institute. At times of difficulty, he has actively pointed me in the right direction, even when he has a busy schedule. His depth of knowledge in various topics never ceases to amaze me. He frequently shares many of his valuable personal experience with his students, which are very useful in our future endeavors. His attention to details has trained me to be my own “reviewer”. Lastly, I appreciate the open environment that Dr. Holdsworth has provided. For these reasons, it has been a privilege to be his student.

I also would to thank my advisory committee, Dr. Ian Welch and Dr. Jeffrey Dixon. In particular, Dr. Welch contributed significantly in my project. Specifically, with his veterinary expertise, he assisted in planning and performing animal surgery. This project would have been impossible without his experience in animal surgery. I thank Dr. Dixon for his help in reviewing my manuscripts and guidance during my graduate studies. In addition to my advisory committee, I would like to thank the following people who also have contributed to my experiment and data analysis. Dr. Stephen Sims, Tom Chrones, and Dr. Kim Beaucage for their assistance in animal care and handling approaches. Dr. Xunhua Yuan for his assistance in x-ray imaging. Hristo Nikolov for his technical assistance on the vibration platform. Steve Pollmann for his assistance in software development. Dr. Joseph Umoh for his assistance in CT scanning. Finally, Jaques Milner for his assistance in data visualization.

As my journey as a graduate student approaches to an end at Robarts, I would like to say that it wouldn't be the same without the wonderful group members of the Dr. Holdsworth's Lab, in no particular order, they are: Chris Norley, Adam Paish, Hristo Nikolov, Justin Tse, Steven Pollmann, Daniel Lorusso, Joseph Umoh, Xunhua Yuan, Dave Edey, Jaques Milner, and Todor Ivanov. Thank you all for putting a smile on my face everyday at Robarts. Thank you Justin for providing me with a ride every Friday for grocery shopping, providing me access to Costco for their free food samples (yum), being an awesome partner in the gym and in online games. I value our friendship greatly. Thank you Chris for being the awesome lab manager that you are. I will never forget the memorable camping trip and the ski trip, which you and Daniel organized. I appreciated the time you spent revising two of my manuscripts. I

know it must have been very painful as my English is terrible. The same can be said for Daniel, who revised this thesis. Also worthy of mention are: Kevin Barker and Jacques Montreuil for being awesome lunch mates, and Matthew Lowerison for being a good friend.

Last but not least, I would like to thank my parents, Lingfang Xu and Xuecheng Hu, who have been supporting me all these years. I wouldn't be at where I am today without their scarifies. Their decision of moving to Canada 15 years ago has changed my life completely. Finally, I would to thank my girlfriend, Jiaying Li, who has been patiently waiting for me to complete my studies in Canada, on the other side of the planet.

# Table of Contents

Abstract .....	ii
Co-Authorship Statement.....	iii
Acknowledgments.....	iv
Table of Contents .....	vi
List of Tables .....	ix
<b>Chapter 1</b> .....	<b>1</b>
1 Introduction.....	1
1.1 Bone physiology .....	1
1.1.1 Bone Remodeling.....	1
1.1.2 Wolff's Law.....	3
1.2 Osteoporosis.....	3
1.3 Whole-Body Vibration.....	5
1.3.1 <i>In Vivo</i> Vibration Quantification .....	7
1.4 Image-Based Approach to <i>In Vivo</i> Vibration Quantification .....	8
1.4.1 Imaging Techniques for Quantifying Vibration .....	9
1.5 Thesis Outline .....	11
References.....	12
<b>Chapter 2</b> .....	<b>17</b>
2 Quantification of mouse <i>in vivo</i> whole-body vibration amplitude from motion-blur using x-ray imaging.....	17
2.1 Introduction.....	17
2.2 Material and methods.....	19
2.2.1 Digital x-ray imaging system.....	19
2.2.2 Vibration Platform .....	21

2.2.3	Motion blur analysis .....	22
2.2.3.1	Motion-induced point spread function .....	22
2.2.3.2	Vibration tracking using fiducial marker beads .....	23
2.2.3.3	Measurement of reference vibration amplitude based on motion blur.....	24
2.2.4	Mouse cage with reference beads .....	25
2.2.5	Surgical implantation of tungsten-carbide fiducial marker beads .....	26
2.2.6	In vivo vibration amplitude measurement based on motion blur .....	27
2.3	Results and Discussion .....	28
2.3.1	The effect of harmonic vibration on beads .....	28
2.3.2	Vibration amplitude measurement and calibration .....	30
2.3.3	In vivo vibration amplitude measurement .....	32
2.4	Conclusion .....	36
	References.....	38
	<b>Chapter 3</b> .....	41
3	Transmission of vertical whole-body vibration in mice .....	41
3.1	Introduction.....	41
3.2	Material and Methods .....	42
3.2.1	Fiducial Markers Implantation.....	43
3.2.2	Imaging System and Processing .....	43
3.2.3	Whole-body Vibration Platform and Mouse Cage .....	44
3.2.4	Vibration Protocols .....	46
3.2.5	Measurement of transmissibility and its dependence on vibration frequency.....	46
3.2.6	Dependence of transmissibility and postures.....	46
3.2.7	Data Analysis .....	48
3.3	Results.....	48

3.4 Discussion.....	52
References.....	56
<b>Chapter 4</b> .....	<b>59</b>
4 Conclusions and Future Directions.....	59
4.1 Summary.....	59
4.2 Limitations and future directions.....	61
4.3 Conclusion.....	63
Reference.....	64
Appendix A: Ethics Approval.....	66
Appendix B: Copyright Permissions.....	67
Curriculum Vitae.....	69

## List of Tables

Table 2-1 Vibration parameters used on bead phantom. ....	24
Table 2-2 Vibration amplitude measured at each implanted region from mouse #1 based on SD ratios.....	36
Table 2-3 Vibration amplitude measured at each implanted region from mouse #2 based on SD ratios.....	36
Table 3-1 Vibration Protocols used in <i>in vivo</i> experiment .....	48

## List of Figures

Figure 1-1 The process of bone remodeling: Osteoclast cells resorb bone mineral. The Osteoblast cells then replenish the bone with new organic matrix that is subsequently mineralized [Reproduced with permission of the SAGE Publication from Lerner <i>et al.</i> , <i>J Dental Res</i> 1:15-21, 2006].	2
Figure 1-2 (a) An osteoporotic bone has degenerated trabecular network due to excess bone resorption, resulting in a decrease of bone structural integrity. (b) A healthy bone has densely populated trabecular network which maintains the structural integrity of the bone [Reproduced with permission of John Wiley & Sons from Dempster <i>et al.</i> , <i>J Bone Miner Res</i> 8:584-595, 2006].	4
Figure 1-3 Whole-body vibration of a mouse. The animal is placed on a platform that moves vertically in a harmonic motion. Three parameters characterized the vibration platform: peak-acceleration (vibration magnitude), vibration amplitude, and vibration frequency.	7
Figure 2-1 Isometric view illustrating the layout of the digital x-ray imaging system and the vibration platform. A) GE Proteus XR-a x-ray unit; B) Electroynamics shaker; C) A CCD camera; D) Scintillating screen, which is comprised of a cut-out from a from Kodak MinR-2 2000 mammographic screen; E) Custom-built mouse cage made of acrylic.	21
Figure 2-2 Whole-body vibration platform for mice	22
Figure 2-3 The custom-designed, acrylic, cage used to minimize the movement of the mouse is shown here magnetically affixed to the vibration platform. Tungsten-carbide reference beads on the sides of the cage serve as fiducial markers to measure the applied, input vibration amplitude.	25
Figure 2-4 Incision into the femur using a 25 gauge hypodermic needle.	27
Figure 2-5 Images of a single reference-bead used to calculate the <i>y-to-x</i> SD ratio at different vibrational amplitudes for calibration: (a) 0 $\mu\text{m}$ ; (b) 78 $\mu\text{m}$ ; (c) 118 $\mu\text{m}$ ; (d) 157 $\mu\text{m}$ ; (e) 196 $\mu\text{m}$ ; (f) 237 $\mu\text{m}$ ; and (g) 277 $\mu\text{m}$ .	29

Figure 2-6 Line profiles across the reference-bead parallel to the y-axis (direction of simple-harmonic motion) for a range of vibration amplitudes. .... 30

Figure 2-7 The characteristic curve of *y-to-x* SD ratios for reference-bead motion-blur at each vibration amplitude (error bars are standard deviation of the mean) used for calibration of the vibration system. .... 31

Figure 2-8 Examples of fitting of a 2-D Gaussian surface to the *in vivo* beads using (5) in order to obtain SD. Note the cubic behavior of the background pixel in both plots. This was due to the close proximity of the bead to the bone. (a) Shows the static case, where there is no vibration. (b) Shows the dynamic case, where vibration is set at 0.43 *g* at 118  $\mu\text{m}$  amplitude..... 33

Figure 2-9 *In vivo* images of implanted beads in mice, under both static conditions and while undergoing whole-body vibration: The bone-implanted beads are outlined in white circles. (a) Static x-ray image of mouse #1 (static conditions); (b) Static x-ray image of mouse #2 (static conditions); (c) WBV x-ray image of mouse #1 at vibration amplitude 118  $\mu\text{m}$ ; (d) WBV x-ray image of mouse #2 at vibration amplitude 118  $\mu\text{m}$ ..... 34

Figure 2-10 (a) *y-to-x* SD ratios for mouse #1 with no vibration (static) and with vibration (dynamic). (b) *y-to-x* SD ratios for mouse #2 with no vibration (static) and with vibration (dynamic). Asterisk denotes statistical significance  $p \leq 0.05$  as compared to the reference bead in the dynamic case in both (a) and (b). .... 35

Figure 3-1 The digital imaging system consists of an x-ray source (A), vibration platform (B), mouse cage (C), scintillating screen (D), and a CCD camera (D). The image system is integrated with a vibration platform so that *in vivo* vibration can be quantified. The x-ray is imaged indirectly; first it is converted into visible photons, via a scintillating screen, which are then captured by a CCD camera. .... 44

Figure 3-2 To prevent the mouse from moving around during imaging, a cage is designed and built such that it limits the animal’s mobility. .... 45

Figure 3-3 The three possible animal postures during imaging are (a) normal standing position, (b) crouch position, and (c) extended leg position..... 47



Figure 3-4 The angle between the femoral and tibial bone is defined by the two imaginary lines drawn through the respective bones as shown. The implanted beads are circled. The femoral line starts at proximal femur and extends longitudinally, through the implanted bead. Similarly, the tibial line starts at the distal tibia and extends longitudinally, through the implanted bead. The angle between the two lines is then measured in ImageJ..... 47

Figure 3-5 An x-ray image of the animal in the restrainer. The implanted beads are highlighted. The scattered beads on the right are the reference beads, which are glued onto the restrainer. Note the elongation of the bead in the vertical direction due to motion blur. . 49

Figure 3-6 The vibration amplitudes of each peak-acceleration category of the same vibration frequency group are plotted. An asterisk denotes statistical significance when compared to the corresponding reference amplitude at the same peak-acceleration and vibration frequency ( $*p < 0.05$  and  $**p < 0.001$ )..... 50

Figure 3-7 The transmissibility values from all the data are plotted against their corresponding tibia-to-femur angle. The transmissibility and animal posture have negative correlation. In the tibia,  $r = -0.2842$ . And,  $r = -0.2993$  in the femur. This suggests that as the angle between the tibial bone and femoral bone decreases, the transmissibility increases. ... 51

Figure 3-8 The transmissibility from the entire peak-acceleration category of the same frequency group are averaged and plotted for each frequency group. The behavior of the transmissibility in the tibia across 15 – 40 Hz range and the behavior of the transmissibility in the femur across 15 – 40 Hz range are shown. Note the increasing transmissibility in the femur in the 15 – 25 Hz range. .... 52

## List of Appendices

Appendix A: Ethics Approval.....	66
Appendix B: Copyright Permissions .....	67

# Chapter 1

## 1 Introduction

Osteoporosis is a degenerative bone disease that affects millions of Canadians each year. In 2010, this disease cost the Canadian economy \$2.3 billion, or 1.3% of Canada's healthcare expenditure.<sup>1</sup> Osteoporosis affects mostly the senior population, of which women are more susceptible than men.<sup>2</sup> The incidence of osteoporotic fractures is greater than that of stroke, breast cancer, and heart attack combined; and the number of those affected by osteoporosis will only continue to rise as baby boomers age. Therefore, the need to develop an effective osteoporosis intervention is greater than ever.

Courtesy of recent advancements in musculoskeletal research, one of the potential, non-pharmaceutical ways of treating and preventing osteoporosis is by exploiting Wolff's Law.<sup>3</sup> This basic idea is that an increase in bone mineral density (BMD) and remodeling of bone architecture, and hence overall bone integrity, can be promoted by introducing an external mechanical stimulation to the entire body of a healthy animal or human. One such way of introducing mechanical stimulation is known as whole-body vibration (WBV), which has shown positive effects in both human and animals.<sup>4-10</sup> The benefit of whole-body vibration extends beyond osteoporosis. For instance, it has been shown to enhance bone-implant integration and fracture healing.<sup>10-12</sup>

### 1.1 Bone physiology

#### 1.1.1 Bone Remodeling

Bones are like the structural steel beams of our body, they allow us to stand up, lift external weights, and grow in physical size. However, it is not commonly known that bone is a dynamic organ on the cellular level. In fact, bone is constantly remodeling itself to repair micro-fractures, replacing old bony tissue, as well as adapting to new local mechanical stresses by increasing BMD and remodeling bone architecture where it is needed.<sup>13-15</sup> Bone remodeling, not to be confused with bone modeling, is a well-orchestrated process. It primarily involves two different cell types, osteoblasts and

osteoclasts. The details of their respective participation in bone remodeling can be summarized in two processes, bone formation and bone resorption.

Osteoclast cells are activated at the site where bone remodeling is taking place.<sup>16</sup> The cells break down the bone matrix by extracting bone minerals such as calcium and phosphorus ions, which get recycled back to the body. This resorption process lasts until the activation and differentiation of osteoblast cells, which replenish the location with new organic matrix that is then mineralized with the inorganic mineral hydroxyapatite (See Fig 1-1). It is important to point out that osteoblast and osteoclast cells travel in a group known as Basic Multicellular Unit (BMU). Its speed averages about 25  $\mu\text{m}$  per day, with osteoclasts leading and osteoblasts trailing. The average lifetime of a BMU is 6 - 9 months, of which bone formation takes up the majority of that time frame.<sup>17</sup>

In a healthy person, the rate of these two processes is roughly equal. Thus, the intricate balance between bone resorption and bone formation keeps the bone healthy and strong.

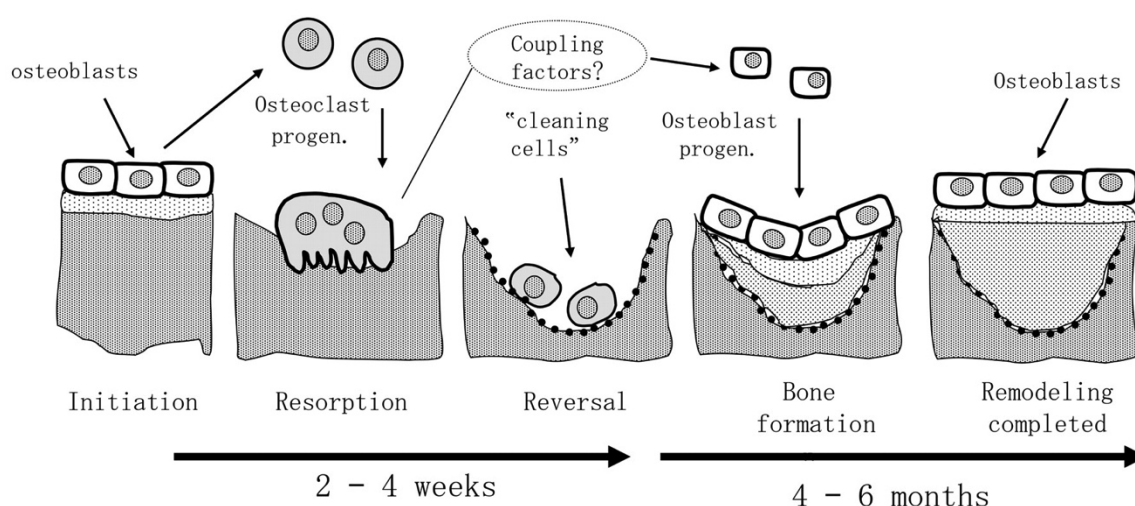


**Figure 1-1** The process of bone remodeling: Osteoclast cells resorb bone mineral. The Osteoblast cells then replenish the bone with new organic matrix that is subsequently mineralized [Reproduced with permission of the SAGE Publication from Lerner *et al.*, *J Dental Res* 1:15-21, 2006].

### 1.1.2 Wolff's Law

Julius Wolff, a German surgeon and anatomist, proposed in 1892 that the bones of humans and animals are constantly adapting to their local mechanical environment. In other words, any external mechanical loading such as pressure, shear, strain, and torque on the bones will induce them to adapt to those mechanical demands accordingly. This is an adaptation analogous to the growth of callus in response to the repetitive friction to the skin.

An example of Wolff's law in action is the loss of bone mass that astronauts experience in space.<sup>18</sup> In a weightless environment, the bones of an astronaut aren't being mechanically subjected to the loading of the astronaut's weight on Earth. This lack of mechanical stimulation triggers the bone to react by resorbing some of the bone mineral, as they are no longer needed and this resource (nutrient) can be better used somewhere else in the body. In contrast, athletes have higher BMD than the average person due to their daily physical training, which stimulates the bone to strengthen itself against the constant mechanical forces induced from exercises.<sup>19</sup>

While the effects of mechanical influence on the bones are known, the exact mechanism of how the bone cells differentiate changes in their mechanical environment (*i.e.* mechanotransduction) is currently unknown and it is an active research topic in the field of mechanobiology.<sup>20,21</sup> There are many theories that are currently being examined in detail, for example, it has been proposed that fluid shear-induced mechanical signaling could be the mechanism.<sup>22,23</sup>

## 1.2 Osteoporosis

In the first two decades of one's life, the rate of bone formation is greater than the rate of resorption, resulting in overall bone growth. The rate approaches equilibrium during mid-life. However, when one approaches the mid-fifties, this process starts to favor bone resorption, *i.e.*, bone loss. Unfortunately, this unbalanced rate only continues to accelerate as one ages. This low BMD leads to a medical condition known as osteoporosis. In addition, post-menopausal women lose bone mass faster than men of the

same age, due to a combined effect of the loss of estrogen and the normal bone aging process.<sup>24</sup> As result, the majority of osteoporosis sufferers are women.

Osteoporosis occurs when there is more bone resorption than bone formation, resulting in the structurally weakening of the bone. The World Health Organization (WHO) defines a BMD below 2.5 standard deviations of the mean BMD in sex-matched, age-matched adults to be osteoporotic.<sup>25</sup> Figure 1-2a and Figure 1-2b show cross-sectional images of iliac crest biopsies from a healthy bone and an osteoporotic bone, respectively.

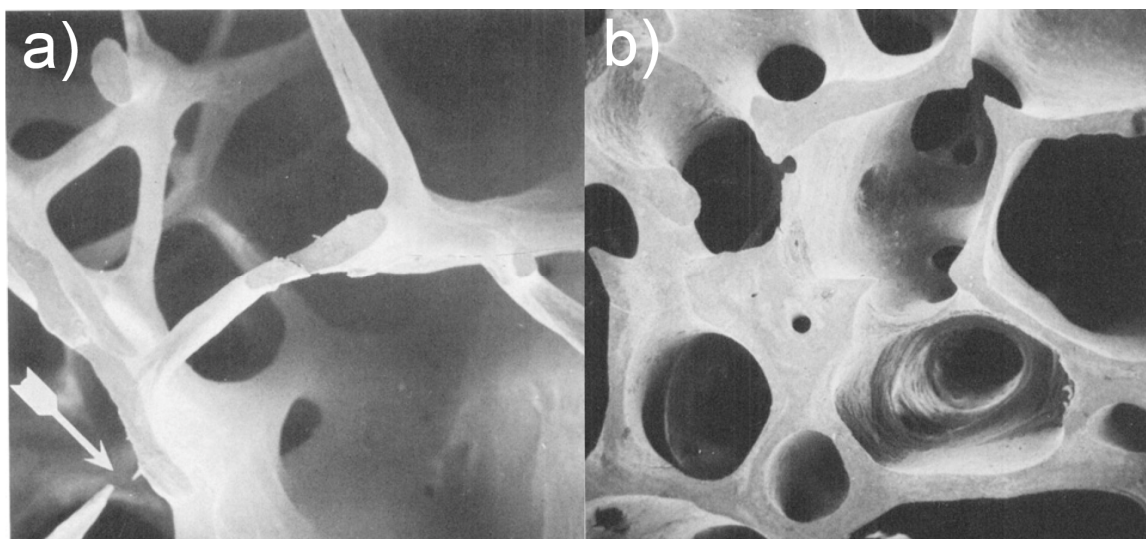


**Figure 1-2** (a) An osteoporotic bone has degenerated trabecular network due to excess bone resorption, resulting in a decrease of bone structural integrity. (b) A healthy bone has densely populated trabecular network which maintains the structural integrity of the bone [Reproduced with permission of John Wiley & Sons from Dempster *et al.*, *J Bone Miner Res* 8:584-595, 2006].

As it is evident, a normal bone has a dense, well-established trabecular (cancellous bone) network. On the other hand, an osteoporotic bone has irregular and highly deteriorated trabecular network, which significantly weakens the structural integrity of the bone. Consequently, the bone is susceptible to fractures, even from a minor physical trauma such as a fall. The quality of life for those who suffer from osteoporosis is greatly affected.

Other than lack of estrogen, as previously mentioned, there are many other factors that could also contribute to osteoporosis. For example, smoking,<sup>26</sup> poor nutrition,<sup>27</sup> and

alcohol abuse.<sup>28</sup> Furthermore, one of the common osteoporotic fractures are hip fractures; in the USA, 1 in 6 osteoporotic fractures can be attributed to the hip.<sup>29</sup> This is significant because mortality rate after hip fracture can be as high as 30%.<sup>30</sup> Interestingly, studies have suggested that men who suffer osteoporotic fracture have higher mortality than women.<sup>31</sup>

Current treatment of osteoporosis primarily utilizes drug-therapy. In particular, bisphosphonates, estrogen therapy, and parathyroid hormone (PTH) are some of the commonly used drug therapies. They specifically target osteoclasts, so that the bone resorption process is stopped or slowed down. Thus, activity from osteoblasts, which are responsible for bone formation, is favored. However, some of them may have long-term side effects. For instance, studies have shown that bisphosphonate, in rare cases, could cause osteonecrosis of the jaw (ONJ).<sup>32</sup> Non-pharmacological treatment of osteoporosis also exists commonly as exercises and improved diet.

### 1.3 Whole-Body Vibration

As mentioned previously, the current pharmaceutical treatment of osteoporosis may induce long-term negative side-effects. Therefore, finding an effective way of reversing bone loss without compromising its natural remodeling processes would be an ideal way of treating osteoporosis. The fact that the bone is sensitive to external mechanical influence, as described in Wolff's Law, has been proposed as a non-pharmaceutical way of preventing, or even reversing, osteoporosis.<sup>6</sup>

Whole-body vibration (WBV) stimulates the bone by introducing a low-amplitude mechanical vibration to the entire body of a person (or an animal) through the feet. In a way, it can be imagined to be like experiencing a miniaturized earthquake. The vibration is also cyclic in nature, *i.e.*, in a sinusoidal waveform. However, not all vibration parameters are thought to be healthy for the musculoskeletal system. In fact, high magnitude and prolonged exposure to vibration can cause tissue damage. The International Standards Organization (ISO) has published a guideline (ISO-2631-1),<sup>33</sup> in which the recommended daily exposures to vertical vibration of different frequencies as function of magnitude, measured as acceleration in  $\text{m/s}^2$ .

The guideline recommends that for vibration at 1 Hz with an acceleration of 0.5  $g$ , where  $g$  is the Earth's gravitational acceleration  $9.8 \text{ m/s}^2$ , exposure to be less than one minute. For higher peak-acceleration (magnitude) for a given vibration frequency, the less time one should be exposed to it.

One of the symptoms of prolonged exposure to vibration magnitude  $\gg 1 g$  is known as the Vibration-Induced White Finger, a symptom frequently occurs to workers who use power tools such as a jackhammer, or other non-powered tools such as a hammer.<sup>34-38</sup> The syndrome is characterized by the distinct pale appearance of one's hand, which is the result of damaged microvasculature.<sup>39</sup> In addition, high intensity vibration encountered in the industrial setting could cause bone and joint damage.<sup>40,41</sup> Finally, research also suggests that high amplitude vibration may be potentially catabolic to bone.<sup>42</sup>

Currently, the literature suggests that high frequency (10-100 Hz), low-magnitude ( $< 1 g$ ) WBV is anabolic in animal and humans.<sup>7,12,42-45</sup> The relationship between peak-acceleration, vibration amplitude, and vibration frequency is shown below, where “A” is the vibration amplitude, “a” is the peak-acceleration, and “f” is the vibration frequency.<sup>46</sup>

$$A = \frac{a}{4\pi^2 f^2} \quad (1)$$

It's important to note that the term “*vibration amplitude*” in WBV is referring to half of the peak-to-peak amplitude.

Given the 10-100 Hz vibration frequency range and the sub 1  $g$  in peak-acceleration, the vibration amplitude in a small-animal WBV experiment is on the order of microns. An illustration of WBV of a mouse is shown in Figure 1-4. The mouse is placed on a vibration platform with its four limbs in full contact with the platform.



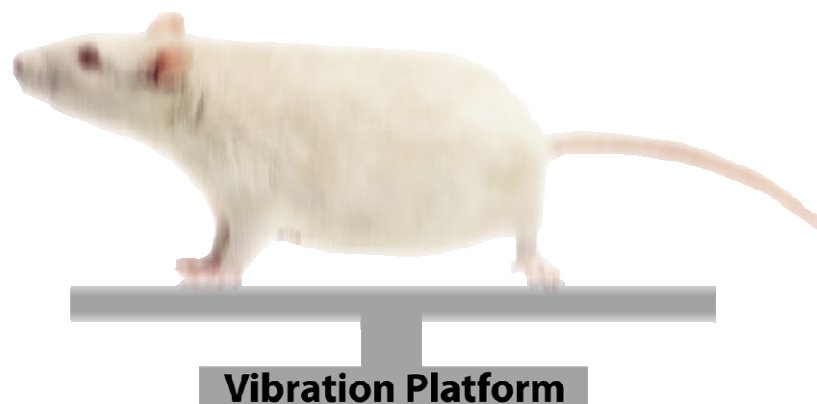


**Figure 1-3** Whole-body vibration of a mouse. The animal is placed on a platform that moves vertically in a harmonic motion. Three parameters characterized the vibration platform: peak-acceleration (vibration magnitude), vibration amplitude, and vibration frequency.

It is worth noting that there are currently conflicted reports as to what set of vibration frequency, peak-acceleration, and vibration amplitude would yield the optimal anabolic bone response. In fact, there are studies that have reported no effects of WBV on the bone of animals and humans, even using vibration protocols which previously have shown to cause positive response.<sup>47-51</sup> Some of the discrepancies could be attributed to different animal strains, sex, age, physiology, and the location of skeletal evaluation used among the studies. However, it remains unknown whether there is a universal WBV protocol that could be applied to all cases, or that the protocol is dependent on the age group, sex, and specific bone of the subject.

### 1.3.1 *In Vivo* Vibration Quantification

While the effects of WBV can be quantified in humans and animals precisely, the amount of vibration transmitted into the bone is also an interest to researchers. It is typical to attach inertia sensors, such as accelerometers, directly onto the skin in human subjects.<sup>52-54</sup> However, soft tissues of various densities surround bones. Thus, vibration at the skin level is attenuated and does not truly reflect the magnitude in the bone, as studies have shown.<sup>55,56</sup> Fortunately, this challenge is relatively easy to overcome in the human subjects. By using Kirschner wire, accelerometers can be attached directly to the bone and this method has been used to quantify transmission of vertical vibration in humans.<sup>57</sup>

There have not been any direct measurements of transmission of vertical vibration in small-animals models like rats and mice, which are often used in musculoskeletal research due to their availability, life span, and similar skeletal response. Previous studies have attempted to quantify the transmission only at the skin-level of a rat using a non-inertial method.<sup>58</sup> Even then, the animal has to be sedated. Otherwise, the motion of the animal would affect the measured acceleration from the accelerometer, which is attached onto the animal. The two major issues with this setup, first, as mentioned before the vibration measured at the skin level does not accurately reflect the magnitude at the skeletal level. Second is that the animal is in a sedate state, which implies that its limbs aren't be mechanically loaded. This affects how vibration is transmitted to its body. In an even smaller animal such as mice, even vibration quantification at the skin level is difficult. This is primarily due to technical limitations. Specifically, the size and the weight of the accelerometer are comparable to the size and weight of the animal. Thus, it would be a significant weight bearing on the animal. Therefore, there is a need to develop a method of characterizing the transmission of vertical vibration in small-animal models.

The amount of vibration transmitted into the bone is an important quantity to know. As mentioned previously, it is not exactly known how bone cells sense mechanical stresses. Hence, if one could characterize the transmission of vibration in bones, then it would provide researchers an estimate of how much vibration is transmitted into to the bone, which in turn will have a direct influence at the cellular level where bone transformation is taken place. Furthermore, because of the difference in the profile of each bone and its position in the body, each one attenuates vibration transmission differently. Lastly, being able to quantify vibration transmission would facilitate the development of appropriate vibration protocols for small-animal models.

## 1.4 Image-Based Approach to *In Vivo* Vibration Quantification

It is clear that using sensor-based approach would not be suitable to quantify *in vivo* vibration in a mouse-model with currently available accelerometers. Perhaps, a more feasible way is to use an image-based approach. In addition, due to the challenges presented in small animal WBV, this image-based method must satisfy two criteria. First,

it should have image resolution at least on the order of micron, since that is the common WBV amplitude in small-animal models. Second, because we are only interested in the transmission of vibration to the skeletal system of the animal, the image-based method must be able to produce good contrast on the skeletal structures. There are 3 types of imaging modalities that are able to image the bone: x-ray imaging, magnetic resonance imaging (MRI), and nuclear imaging. However, MRI and nuclear imaging cannot be used in this case due to their lack of imaging resolution (on the order of millimeter) and other reasons such as long acquisition time (on the order of minutes). This particular factor is troublesome, since we would like to keep the animal unsedated. As a result, prolonged acquisition time is susceptible to motion artifacts. On the other hand, x-ray imaging has the ability to attain sub-millimeter resolution, given the right detector and optical setup. Most importantly, bone is the most prominent feature in an x-ray image due to its attenuation of the x-ray beam, in the absence of metallic object.

The detection of x-rays can be classified into two categories, direct and indirect. The former converts x-ray photons to electrical signal directly, which is then converted into digital signal and fed into a computer. This method of detection has become the norm due to the recent advancement of solid-state detectors and computers. The indirect method first converts the x-ray into visible photons, via a scintillating screen, which are then captured by a camera. While this particular method of x-ray imaging is easy to set up relative to the direct imaging method, it suffers from minor degradation in signal and resolution due to extra conversion processes. These defects can be a concern, but are negligible in most cases.

#### 1.4.1 Imaging Techniques for Quantifying Vibration

One other consideration is the appropriate technique for quantifying vibration through x-ray imaging. It should be noted first that WBV is a form of simple harmonic motion. Its motion can be described by a sine wave. Consequently, there are three ways in which one can quantify a simple harmonic motion: high-speed imaging and time-exposure imaging.

High-speed imaging utilizes fast sampling such that the rate of sampling is greater than the Nyquist frequency, which is two times of the highest vibration frequency, in order to

avoid aliasing. The high sampling rate can be done with an imaging detector capable of attaining high frame rate. For instance, if one would like to use high speed imaging to characterize 45 Hz vibration, one would need to sample it at least 90 Hz, or 90 frames per second. While there are many high-speed cameras available on the market and they are more than capable of capturing at high frame rate, the limitation is amount of x-ray flux that can be captured in each frame. For example, at 90 frames per second each frame is exposed for 11 milliseconds. For higher vibration frequency, the exposure time will only decrease. Thus, this factor severely affects the image quality due to lack of x-ray photon flux.

Finally, time-exposure imaging, or long exposure imaging, is a method based on sampling a periodic motion much longer than its period. While this particular method is able to capture the entire range of motion of vibration, it loses temporal information. This is because during sampling the motion is repeated over several cycles, thus any temporal information, such as frequency, is blurred out. However, information regarding vibration amplitude is preserved, which is the goal in quantifying vibration *in vivo*. One advantage associated with long exposure imaging is that it allows sufficient amount of photon flux into the detector. However, by prolong sampling time it also causes image more susceptible to motion artifacts. But, a trade off can be made between photon flux and susceptibility to motion artifact in term of sampling rate.

It should be noted that vibration quantification via time-exposure imaging would only work if the detector were tracking a particle, since the blur of the particle due to simple harmonic motion is clearly distinguishable and its intensity profile can be easily modeled. Biological features, such as bone, are difficult to model consistently. This issue can be addressed by implanting metallic fiducial markers in the skeleton of the animal. Moreover, the metallic fiducial marker would be even more prominent in an x-ray image due to the fact that it's much denser than bone. Therefore, time-exposure imaging of vibrating fiducial markers could be a potential candidate in quantifying *in vivo* vibration.

## 1.5 Thesis Outline

The aim of this thesis was to develop a novel image-based method to quantify vibration *in vivo* in small-animal models. This approach is based on the implantation of small metallic fiducial markers within the skeleton of the subject animal. These marker beads can then be recorded non-invasively by x-ray imaging during whole-body vibration. The challenge presented here is that the frequency of the vibration is relatively high, which would require a high-speed (i.e. greater than 90 Hz), low-noise fluoroscopic imaging sequence to characterize bead motion accurately. This may not be technically feasible, due to limitations in the available x-ray flux. An alternative approach, which is the topic of this thesis, is to use longer x-ray exposures and deliberately allow the image of the marker bead to blur. Careful image post-processing can then be used to characterize the motion blur and correlate it with the amplitude of vibration.

Chapter 2 describes the development of such a digital planar x-ray imaging system, as well as an image processing technique that was capable of quantifying *in vivo* skeletal vibration using x-ray projection images.

Chapter 3 describes the application of this technique *in vivo* by characterizing the transmission of vertical vibration in mice. For both of these studies, the x-ray imaging system had to be integrated with a customized whole-body vibration platform for mice, making an indirect x-ray imaging approach the most feasible design for this project.

## References

- (1) Tarride, J. E. *et al.* The burden of illness of osteoporosis in Canada. *Osteoporosis Int* **23**, 2591-2600, (2012).
- (2) Melton, L. J., Chrischilles, E. A., Cooper, C., Lane, A. W. & Riggs, B. L. How Many Women Have Osteoporosis. *J Bone Miner Res* **7**, 1005-1010, (1992).
- (3) Wolff, J. *Das Gesetz der Transformation der Knochen (The Law of Bone Remodelling)*. (Berlin: Verlag von August Hirschwald, 1892).
- (4) Verschueren, S. M. P. *et al.* Effect of 6-month whole body vibration training on hip density, muscle strength, and postural control in postmenopausal women: A randomized controlled pilot study. *J Bone Miner Res* **19**, 352-359, (2004).
- (5) Wenger, K. H. *et al.* Effect of whole-body vibration on bone properties in aging mice. *Bone* **47**, 746-755, (2010).
- (6) Rubin, C., Judex, S. & Qin, Y.-X. Low-level mechanical signals and their potential as a non-pharmacological intervention for osteoporosis. *Age Ageing* **35 Suppl 2**, ii32-36, (2006).
- (7) Gilsanz, V. *et al.* Low-level, high-frequency mechanical signals enhance musculoskeletal development of young women with low BMD. *J Bone Miner Res* **21**, 1464-1474, (2006).
- (8) Judex, S., Lei, X., Han, D. & Rubin, C. Low-magnitude mechanical signals that stimulate bone formation in the ovariectomized rat are dependent on the applied frequency but not on the strain magnitude. *J. Biomech.* **40**, 1333-1339, (2007).
- (9) Kasturi, G. & Adler, R. A. Mechanical Means to Improve Bone Strength: Ultrasound and Vibration. *Current rheumatology reports* **13**, 251-256, (2011).
- (10) Stuermer, E. K. *et al.* Musculoskeletal response to whole-body vibration during fracture healing in intact and ovariectomized rats. *Calcified Tissue Int* **87**, 168-180, (2010).
- (11) Mavčič, B. & Antolič, V. Optimal mechanical environment of the healing bone fracture/osteotomy. *International Orthopaedics (SICOT)* **36**, 689-695, (2012).
- (12) Chen, B., Li, Y., Xie, D. & Yang, X. Low-magnitude high-frequency loading via whole body vibration enhances bone-implant osseointegration in ovariectomized rats. *Journal of Orthopaedic Research* **30**, 733-739, (2012).
- (13) Hadjidakis, D. J. & Androulakis, II. Bone remodeling. *Annals of the New York Academy of Sciences* **1092**, 385-396, (2006).

- (14) Cowin, S. C. & Hegedus, D. H. Bone Remodeling .1. Theory of Adaptive Elasticity. *J. Elast.* **6**, 313-326, (1976).
- (15) Lanyon, L. E., Goodship, A. E., Pye, C. J. & Macfie, J. H. Mechanically Adaptive Bone Remodeling. *J. Biomech.* **15**, 141-154, (1982).
- (16) Boyle, W. J., Simonet, W. S. & Lacey, D. L. Osteoclast differentiation and activation. *Nature* **423**, 337-342, (2003).
- (17) Parfitt, A. M. Osteonal and Hemi-Osteonal Remodeling - the Spatial and Temporal Framework for Signal Traffic in Adult Human Bone. *J. Cell. Biochem.* **55**, 273-286, (1994).
- (18) LeBlanc, A. *et al.* Bone mineral and lean tissue loss after long duration space flight. *Journal of musculoskeletal & neuronal interactions* **1**, 157-160, (2000).
- (19) Ducher, G., Bass, S. L., Saxon, L. & Daly, R. M. Effects of repetitive loading on the growth-induced changes in bone mass and cortical bone geometry: A 12-month study in pre/peri- and postmenarcheal tennis players. *J Bone Miner Res* **26**, 1321-1329, (2011).
- (20) Rubin, J., Rubin, C. & Jacobs, C. R. Molecular pathways mediating mechanical signaling in bone. *Gene* **367**, 1-16, (2006).
- (21) Wang, J. H. C. & Thampatty, B. P. An introductory review of cell mechanobiology. *Biomech. Model. Mechanobiol.* **5**, 1-16, (2006).
- (22) Pavalko, F. M. *et al.* Fluid shear-induced mechanical signaling in MC3T3-E1 osteoblasts requires cytoskeleton-integrin interactions. *The American journal of physiology* **275**, C1591-1601, (1998).
- (23) Gardinier, J. *et al.* P2Y2 receptors regulate osteoblast mechanosensitivity during fluid flow. *American journal of physiology. Cell physiology* **306**, C1058-1067, (2014).
- (24) Compston, J. E. Sex steroids and bone. *Physiological reviews* **81**, 419-447, (2001).
- (25) Kanis, J. A. Assessment of fracture risk and its application to screening for postmenopausal osteoporosis: synopsis of a WHO report. WHO Study Group. *Osteoporosis Int* **4**, 368-381, (1994).
- (26) Wong, P. K., Christie, J. J. & Wark, J. D. The effects of smoking on bone health. *Clinical science* **113**, 233-241, (2007).
- (27) Gloth, F. M., 3rd, Smith, C. E., Hollis, B. W. & Tobin, J. D. Functional improvement with vitamin D replenishment in a cohort of frail, vitamin D-deficient older people. *J Am Geriatr Soc* **43**, 1269-1271, (1995).

- (28) Felson, D. T., Kiel, D. P., Anderson, J. J. & Kannel, W. B. Alcohol consumption and hip fractures: the Framingham Study. *American journal of epidemiology* **128**, 1102-1110, (1988).
- (29) Riggs, B. L. & Melton, L. J., 3rd. The worldwide problem of osteoporosis: insights afforded by epidemiology. *Bone* **17**, 505S-511S, (1995).
- (30) Goldacre, M. J., Roberts, S. E. & Yeates, D. Mortality after admission to hospital with fractured neck of femur: database study. *BMJ (Clinical research ed.)* **325**, 868-869, (2002).
- (31) Panula, J. *et al.* Mortality and cause of death in hip fracture patients aged 65 or older: a population-based study. *BMC musculoskeletal disorders* **12**, 105, (2011).
- (32) Marx, R. E. Pamidronate (Aredia) and zoledronate (Zometa) induced avascular necrosis of the jaws: a growing epidemic. *Journal of Oral and Maxillofacial Surgery* **61**, 1115-1117, (2003).
- (33) International Organization for Standardization Section. Number Mechanical Vibration and Shock - Evaluation of Human Exposure to Whole-Body Vibration - Part 1: General Requirement, Geneva, Switzerland: International Organization for Standardization, 1997.
- (34) Bovenzi, M., Franzinelli, A. & Strambi, F. Prevalence of Vibration-Induced White Finger and Assessment of Vibration Exposure among Travertine Workers in Italy. *International Archives of Occupational and Environmental Health* **61**, 25-34, (1988).
- (35) Griffin, M. J. & Bovenzi, M. The diagnosis of disorders caused by hand-transmitted vibration: Southampton Workshop 2000. *International Archives of Occupational and Environmental Health* **75**, 1-5, (2002).
- (36) Starck, J., Jussi, P. & Ilmari, P. Physical Characteristics of Vibration in Relation to Vibration-Induced White Finger. *American Industrial Hygiene Association Journal* **51**, 179-184, (1990).
- (37) Behrens, V. *et al.* Vibration Syndrome in Chipping and Grinding Workers. *Journal of Occupational and Environmental Medicine* **26**, 765-788, (1984).
- (38) Yu, Z. S., Chao, H., Qiao, L., Qian, D. S. & Ye, Y. H. Epidemiologic Survey of Vibration Syndrome among Riveters, Chippers and Grinders in the Railroad System of the Peoples-Republic-of-China. *Scand. J. Work Environ. Health* **12**, 289-292, (1986).
- (39) Takeuchi, T., Futatsuka, M., Imanishi, H. & Yamada, S. Pathological-Changes Observed in the Finger Biopsy of Patients with Vibration-Induced White Finger. *Scand. J. Work Environ. Health* **12**, 280-283, (1986).



- (40) Bovenzi, M. Health effects of mechanical vibration. *Giornale italiano di medicina del lavoro ed ergonomia* **27**, 58-64, (2005).
- (41) Schenk, T. Statistical analysis of vibration-induced bone and joint damages. *Central European journal of public health* **3 Suppl**, 113-117, (1995).
- (42) Turner, S. *et al.* A randomized controlled trial of whole body vibration exposure on markers of bone turnover in postmenopausal women. *Journal of osteoporosis* **2011**, 710387, (2011).
- (43) Tezval, M. *et al.* Improvement of femoral bone quality after low-magnitude, high-frequency mechanical stimulation in the ovariectomized rat as an osteopenia model. *Calcif Tissue Int* **88**, 33-40, (2011).
- (44) Rubin, C. *et al.* Prevention of postmenopausal bone loss by a low-magnitude, high-frequency mechanical stimuli: A clinical trial assessing compliance, efficacy, and safety. *J Bone Miner Res* **19**, 343-351, (2004).
- (45) McCann, M. R. *et al.* Acute vibration induces transient expression of anabolic genes in the murine intervertebral disc. *Arthritis Rheum* **65**, 1853-1864, (2013).
- (46) Griffin, M. J. *Handbook of human vibration*. (Academic Press, 1990).
- (47) Lynch, M. A., Brodt, M. D. & Silva, M. J. Skeletal effects of whole-body vibration in adult and aged mice. *Journal of Orthopaedic Research* **28**, 241-247, (2010).
- (48) Nowak, A., Lochynski, D., Pawlak, M., Romanowski, W. & Krutki, P. High-magnitude whole-body vibration effects on bone resorption in adult rats. *Aviation, space, and environmental medicine* **85**, 518-521, (2014).
- (49) Slatkowska, L. *et al.* Effect of 12 months of whole-body vibration therapy on bone density and structure in postmenopausal women: a randomized trial. *Annals of internal medicine* **155**, 668-679, W205, (2011).
- (50) Torvinen, S. *et al.* Effect of 8-month vertical whole body vibration on bone, muscle performance, and body balance: a randomized controlled study. *J Bone Miner Res* **18**, 876-884, (2003).
- (51) Lau, R. W. *et al.* The effects of whole body vibration therapy on bone mineral density and leg muscle strength in older adults: a systematic review and meta-analysis. *Clinical rehabilitation* **25**, 975-988, (2011).
- (52) Kiiski, J., Heinonen, A., Jaervinen, T. L., Kannus, P. & Sievanen, H. Transmission of vertical whole body vibration to the human body. *J Bone Miner Res* **23**, 1318-1325, (2008).

- (53) Crewther, B., Cronin, J. & Keogh, J. Gravitational forces and whole body vibration: implications for prescription of vibratory stimulation. *Phys. Ther. Sport* **5**, 37-43, (2004).
- (54) Morgado Ramírez, D. Z., Strike, S. & Lee, R. Y. W. Measurement of transmission of vibration through the human spine using skin-mounted inertial sensors. *Med. Eng. Phys.* **35**, 690-695, (2013).
- (55) Nokes, L., Fairclough, J. A., Mintowt-Czyz, W. J., Mackie, I. & Williams, J. Vibration analysis of human tibia: the effect of soft tissue on the output from skin-mounted accelerometers. *Journal of biomedical engineering* **6**, 223-226, (1984).
- (56) Ziegert, J. C. & Lewis, J. L. The Effect of Soft Tissue on Measurements of Vibrational Bone Motion by Skin-Mounted Accelerometers. *Journal of Biomechanical Engineering* **101**, 218-220, (1979).
- (57) Rubin, C. *et al.* Transmissibility of 15-hertz to 35-hertz vibrations to the human hip and lumbar spine: determining the physiologic feasibility of delivering low-level anabolic mechanical stimuli to skeletal regions at greatest risk of fracture because of osteoporosis. *Spine* **28**, 2621-2627, (2003).
- (58) Holguin, N., Uzer, G., Chiang, F. P., Rubin, C. & Judex, S. Brief daily exposure to low-intensity vibration mitigates the degradation of the intervertebral disc in a frequency-specific manner. *Journal of Applied Physiology* **111**, 1846-1853, (2011).

## Chapter 2

*In preparation for submission to the journal of Physics in Medicine and Biology*

## 2 Quantification of mouse *in vivo* whole-body vibration amplitude from motion-blur using x-ray imaging

### 2.1 Introduction

Osteoporosis is a bone disease characterized by the loss of bone mineral density (BMD). As a result, individuals suffering from this disease are highly susceptible to bone fractures, even from a relatively minor trauma such a fall. With an increasingly ageing population, the financial burden on the healthcare system of treating osteoporosis will continue to rise. One potential non-pharmacological treatment for reversing and preventing osteoporosis is the use of low-level mechanical stimulation to stimulate bone growth.<sup>1,2</sup> This treatment is based on the principle of Wolff's law,<sup>3</sup> which states that the bones of human and animal are constantly adapting to its local mechanical environment such as pressure, shear stress, and strain. Consequently, bone is constantly remodeled itself resulting in increased or decreased BMD, depending on the mechanical requirements of its local environment. One dramatic manifestation of Wolff's Law is the case of astronauts in space,<sup>4</sup> where their BMD decreases significantly due to lack of mechanical stimulation and decreased load bearing in a micro-gravity environment.

One way of introducing mechanical stimulation to the body is the whole-body vibration (WBV), which applies a carefully controlled mechanical vibration to the entire body of a human or animal through the feet. Many positive effects of WBV have been reported, both in human studies<sup>5-9</sup> and animal studies.<sup>10-14</sup>

WBV is characterized by three key parameters: peak-acceleration, vibration frequency, and vibration amplitude. It is important to note that not all vibrational parameter combinations are healthy to the musculoskeletal system. Prolonged exposure to high peak-acceleration vibration has been shown to cause micro-vascular damage in the hands.<sup>15-17</sup> Therefore, in order to promote bone growth, the common range of vibration

parameters used in animals studies are frequencies from 15 - 90 Hz, and peak-accelerations of 0.1 - 1.0 g, where g is the Earth's gravitational acceleration ( $9.81 \text{ m/s}^2$ ). These parameters result in amplitudes on the order of a few microns to approximately 1 millimeter.

While the effects of WBV are well documented, direct and quantitative measurement of the degree to which vibration is transmitted through the skeletal system from a vibration platform has not been reported, especially for small animals such as mice.

In humans, WBV studies have previously reported the transmitted vibration at the skin level via skin-mounted accelerometers at regions of interest<sup>18-20</sup>. However, it has been noted that the vibration measured at the skin level does not truly reflect that experienced at the skeletal level<sup>21,22</sup>. This problem has been overcome in human cases by Rubin *et al.*,<sup>23</sup> who employed Kirschner-wire inserted onto the proximal femur and lumbar vertebrae of the subject. The wires act as a platform from which accelerometers are attached, effectively "anchoring" the accelerometers to the bone and allowing the transmitted vibration to be accurately measured.

In murine studies, attaching currently available, relatively heavy accelerometers to the skin or directly to the bone introduces significant weight-loading to the relatively-small animal, which alters its biomechanics and ultimately vibration transmission. Most importantly, it is unlikely for a mouse to stand still sufficiently long enough for accurate measurements. As a result, a different measuring technique is needed. Holguin *et al.*<sup>24</sup> used Computer Aided Speckle Interferometer (CASI) to measure the transmitted vibration at the skin-level of a rat. There is no currently available technique for measuring the transmitted vibration directly at the skeletal level in small animals, such as rats or mice.

In this chapter a novel image-based technique is presented to quantify sinusoidal WBV and skeletal transmission in mice using x-ray imaging. This technique is insensitive to image quality degradation resulting from the relative motion of the subject and the imaging detector. In fact, we exploit this measurable blur in order to quantify the vibration. We validate our technique *in vivo* using a custom x-ray imaging system,

vibration platform, and post-processing software. The following discussion will first introduce the imaging system, the principle of motion blur and its basic formulation. Initial *in vivo* results are also presented.

## 2.2 Material and methods

### 2.2.1 Digital x-ray imaging system

The imaging system used in all of our experiments is integrated with a custom-built mouse vibration platform, which is described in detail in the following section. An x-ray beam with peak energy of 80 kV<sub>p</sub>, tube-current of 200 mA, and 630 millisecond exposure is passed through an animal standing on the vibration platform and converted to visible light using a mammographic screen (MinR-2 2000, Kodak, Rochester, NY) as a scintillating material. A CCD camera then captures the resultant visible-light image from the scintillating material. Note that there are two ways in which images can be captured from the scintillating screen, from the front of the screen and from the back of the screen. In our setup, the CCD camera is setup so that it captures the image from the front of the scintillating screen. This is done because of two reasons. First, if the CCD were to place behind the screen, it would be in direct line-of-sight with the x-ray tube. As result, high energy x-ray photons would not only affect the image quality in the form of white noise, but also they may cause permanent damage to the CCD chip, resulting in “dead pixels”. This problem could be resolved by placing a lead glass in between the CCD and the screen. However, the optical quality of a lead glass is generally poor, since it is not designed as an optical component. Lastly, image resolution from the back of the scintillating screen is poor compared to the front due to the nature of the scintillating screen.

The CCD camera (Cascade 1K, Photometrics, Tucson, AZ) has an overall 1002 x 1004 pixel resolution, with 8 μm pixel spacing. This camera was chosen not only because of its capability of high resolution imaging, but also the fact that it is capable of acquiring data in a very low-light environment, with negligible readout noise, due to its electron-multiplying (EM) technology. A C-mount thread on the face of the CDD camera enables it to accept various standard camera lenses. The CCD camera is mounted 40 cm away

from the scintillating screen, measured from the CCD plane. The plane of the scintillating screen is parallel with the CCD plane. We chose a Nikkor 50 mm f/1.4 lens (Nikon, Tokyo, Japan), which results in good light-gathering properties. The entire imaging system is enclosed in a light-tight enclosure to reduce confounding ambient light from entering the system and maximize the intensity and contrast from the scintillating screen.

The CCD camera is shielded by approximately 5 mm of lead foil on the side adjacent to the x-ray source in order to minimize direct interaction of stray x-ray photons incident on the CCD chip. These x-ray photons result in spurious, bright, white pixels on the acquired image and potential damage to the detector.

Image acquisition and camera control are performed using Micro-Manager Open Source Microscope Software ([www.micro-manager.org](http://www.micro-manager.org)).

A bird's eye view schematic of the complete system is shown in Figure 2-1. X-rays are generated from a ceiling mounted unit (Proteus XR-a, GE Medical Systems, Milwaukee, WI, USA). At the centre of the platform is a mouse cage, which would be discussed in detail later on. The distance from the focal spot to the centre of the vibration platform is 65 cm. The centre of the platform to the scintillating screen is 28 cm.

Due to the orientation of the vibration platform and the x-ray source, the plane of the scintillating screen is tilted  $32^\circ$  from the normal, relative to the x-ray beam. Therefore, images generated are geometrically stretched in the horizontal direction. This aberration can be rectified using a tilted-detector correction algorithm<sup>25</sup>, which corrects for any geometric warping by the camera lens and the geometric stretching due to the detector orientation. Briefly, an x-ray image of an evenly spaced (4 mm) metallic bead grid, placed at the centre of the platform, was obtained. The image was then used to map the distorted spatial distance to the correct spatial distance, since the grid is evenly spaced.

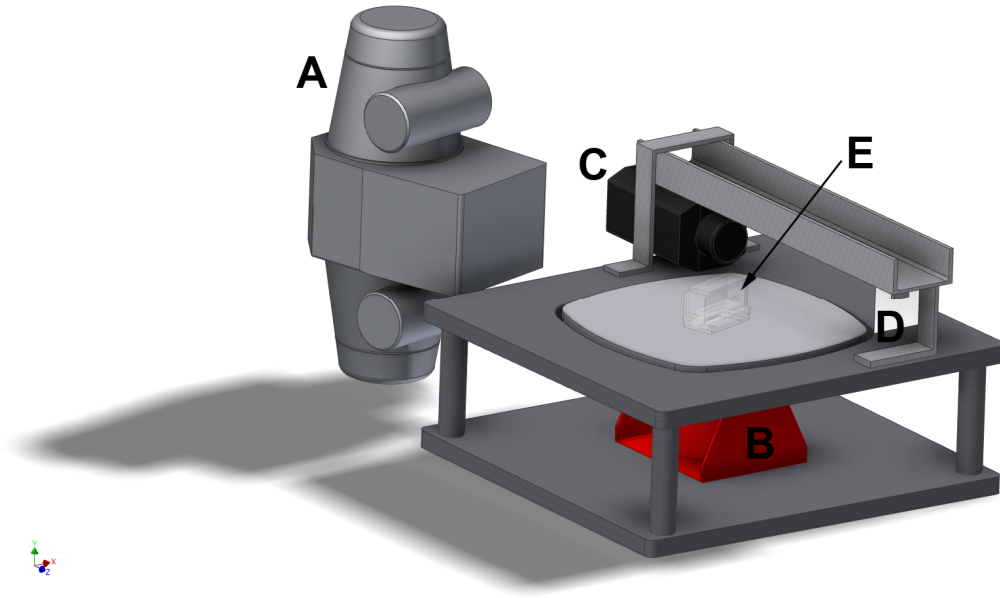


**Figure 2-1** Isometric view illustrating the layout of the digital x-ray imaging system and the vibration platform. A) GE Proteus XR-a x-ray unit; B) Electrodynamic shaker; C) A CCD camera; D) Scintillating screen, which is comprised of a cut-out from a Kodak MinR-2 2000 mammographic screen; E) Custom-built mouse cage made of acrylic.

## 2.2.2 Vibration Platform

The custom-built vibration platform designed to study the effects of WBV on mice is shown in Figure 2-2. The system consists of the following main components: 1) a function generator (Model 148A, WaveTek, AeroFlex, Plainview, NY) which generates a sinusoidal control signal at the desired frequency; 2) a 100-watt power amplifier (Signal Force, Data Physics Corp., San Jose, CA) to vary the peak-acceleration and amplitude of the vibration signal; 3) an accelerometer (Model 7500A1, Dytran Inc., Chatsworth, CA) firmly affixed to the vibration platform, to measure the peak-acceleration of the vibration platform; and 4) an electrodynamic shaker (Type V20, Signal Force, Data Physics Corp., San Jose, CA) to mechanically actuate the vibration platform. The voltage output of the accelerometer is converted to  $g$  via the manufacturer-supplied conversion rate.

The interdependence of the amplitude ( $A$ ), peak-acceleration ( $a$ ), and frequency ( $f$ ) of the vibration for a simple-harmonic oscillator is given by equation (1),<sup>26</sup>

$$A = \frac{a}{4\pi^2 f^2} \quad (1)$$

Therefore, if one is interested in studying the effects of vibration at a particular frequency, the peak-acceleration and amplitude must both be varied in order to hold the frequency constant.

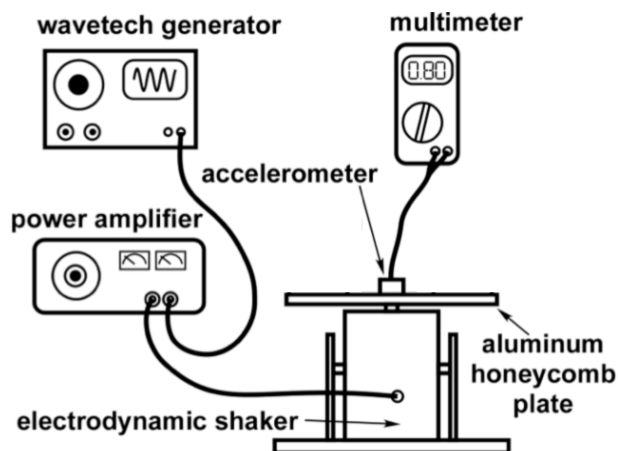


**Figure 2-2** Whole-body vibration platform for mice

The vibrational amplitude produced by the shaker was verified with respect to equation (1) using high-speed (300 frames/second) HD photography, using a Casio Ex-F1 DSLR, of a Cartesian grid of dots of known spatial separation. The dot paper was vibrated with predetermined input amplitudes and the centroid of each dot in each frame was then calculated from the high-speed video data. The centroid positions from each frame were fitted to a sinusoidal curve to calculate the resultant amplitude, which was compared to the requested input amplitude.

## 2.2.3 Motion blur analysis

### 2.2.3.1 Motion-induced point spread function

Since our goal is to quantify simple harmonic vibration (*i.e.* sinusoidal) *in vivo*, it was important to understand how vibration affects image quality. Mathematically, an image,  $I(x,y)$ , is the convolution between the Point Spread Function (PSF) and some object  $F(x,y)$  in the spatial space, assuming noise is negligible. The PSF describes how the object will be modulated in the image space depending on the nature of the optical system and the image detector characterization.



$$I(x, y) = F(x, y) * PSF(x, y) \quad (2)$$

However, when the object moves relative to the imaging detector, there is an additional PSF induced by this relative motion. For the special case of simple-harmonic motion, this PSF can be modeled analytically. Furthermore, since the vibration frequency that is used in WBV has a period much shorter than our imaging time, the analytical model for the simple harmonic motion-induced PSF can be further simplified, as given by Hadar *et al.*,<sup>27</sup>

$$PSF(x) = \frac{1}{\pi\sqrt{L^2 - x^2}}, |x| < L \quad (3)$$

where L is the vibration amplitude. We emphasize that this equation is only valid for CCD acquisition times much longer than period of the vibration, so that the overall blur is due purely to the peak-to-peak cyclic motion caused by the vibration.

### 2.2.3.2 Vibration tracking using fiducial marker beads

Tungsten carbide beads (New England Miniature Ball Company, Norfolk, CT), with diameter of 280  $\mu\text{m}$ , were implanted into the mouse leg at several anatomical locations to serve as fiducial markers for tracking the vibrational motion *in vivo*. The high density of tungsten carbide provides significantly greater contrast than that of bone and the static pixel intensity profile of the bead can be modeled as a 2-D Gaussian surface.

It was necessary to characterize the effects of harmonic motion on the intensity profile of the tungsten-carbide beads before employing this technique *in vivo*. A total of 10 reference beads, 5 per side, were glued to the acrylic cage that would contain the mouse during the experiment. Images of the static beads were acquired in order to characterize the intensity profile of the beads themselves. Images of the motion-blurred beads were acquired as the reference cage was vibrated at a frequency of 30 Hz at various peak-accelerations and amplitudes outlined in Table 2-1. The phantom was imaged 3 times at each peak-acceleration value using x-ray energy of 80 kV<sub>p</sub>, tube current of 200 mA, and 0.63 second long exposure. The 3 images were then averaged and corrected for bright-field, dark-field, and geometric distortion anomalies. A line profile through the

centroid of each bead was plotted at each amplitude, only in the direction of vibration ( $y$ -axis), since the applied vibration blurs the motion only in this direction, as shown in equation (3). During *in vivo* experiments, the cage reference beads also served to measure the applied input vibration amplitude.

**Table 2-1** Vibration parameters used on bead phantom.

	Peak-Acceleration (g)	Amplitude ( $\mu\text{m}$ )
Vibration	0.00	0
Frequency	0.28	78
	0.43	118
(Hz)	0.57	157
	0.71	196
30	0.86	237
	1.00	277

### 2.2.3.3 Measurement of reference vibration amplitude based on motion blur

In general, a Gaussian distribution is defined by its standard deviation (SD). In the case for a 2-D Gaussian surface, it is characterized by both of the SD along orthogonal directions  $x$  and  $y$  in the image space. Thus, the intensity profile of the bead may be fitted to a 2-D Gaussian surface given in equation (4),

$$f(x, y) = A \cdot \exp\left(-\left(\frac{(x - x_0)^2}{2\sigma_x^2} + \frac{(y - y_0)^2}{2\sigma_y^2}\right)\right) + k \quad (4)$$

where  $A$  is maximum pixel intensity,  $x_0$  and  $y_0$  are the centroid coordinates,  $k$  is the background greyscale offset, and  $\sigma_x$  and  $\sigma_y$  are the SD in the  $x$  and  $y$  direction respectively. The approximate centroid of each bead on the image was manually selected to seed an intensity-fitting algorithm, in which a 40 x 40 pixel region centered on the centroid and circumscribing the bead, was fitted to a 2-D Gaussian surface using weighted, non-linear regression. The resultant SD bead widths in both the  $x$  and  $y$  directions are then calculated using MATLAB (MathWorks, Natick, MA) code.

In order to eliminate the dependence of the SD on geometric magnification (the ratio of x-ray source-to-detector distance over the x-ray source-to-subject distance), a ratio was

taken between the SD along the  $y$  and  $x$  directions such that, in the static case, the  $y$ -to- $x$  SD ratio is expected to be 1, to reflect the spherical symmetry of the beads.

#### 2.2.4 Mouse cage with reference beads

Imaging a live, un-anaesthetized mouse, which is in virtually constant motion, is especially troublesome because we are attempting to quantify vibration on the order of microns. In order to minimize motion of the animal, a specially designed acrylic cage, 8.3 cm long x 4.0 cm wide x 3.5 cm height, shown in Figure 2-3, was made to contain and confine the mouse. The width of the cage was made adjustable to accommodate mice of various sizes. Most importantly, the cage confines the mouse in a way that does not apply any physical restraint so there is no additional force applied to the mouse and it retains its natural, unrestricted stance and posture.

The cage was affixed to the vibration platform using neodymium magnets so that it was firmly held in place while maintaining the flexibility to orient it freely.

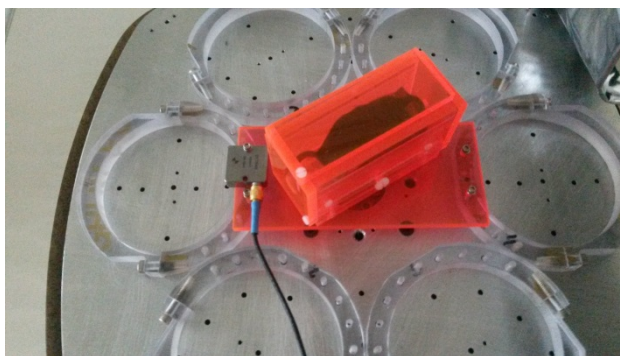


**Figure 2-3** The custom-designed, acrylic, cage used to minimize the movement of the mouse is shown here magnetically affixed to the vibration platform. Tungsten-carbide reference beads on the sides of the cage serve as fiducial markers to measure the applied, input vibration amplitude.

### 2.2.5 Surgical implantation of tungsten-carbide fiducial marker beads

All procedures were approved by the University of Western Ontario's Animal Use Subcommittee and were conducted in accordance with guidelines set out by the Canadian Council on Animal Care. Both mice (N = 2) used in the experiments were three-month old, male, C57BL/6J mice with weights of 25 g. The mice are anaesthetized in an induction chamber with 4% isoflurane then maintained on a nose cone with 2% isoflurane. An anti-inflammatory agent, Meloxicam, 0.01 ml/kg (Boehringer Ingelheim Vetmedica Inc., St. Joseph, MO) was administered prior to surgery.

Two different surgical implantation techniques were assessed for the measurement of vibration amplitude using *in vivo* tungsten-carbide fiducial marker beads: 1) submuscular - placing the bead on the surface of the bone just under the major muscle group; and 2) intraosseous - drilling a hole through the cortical shell and placing the bead into the cancellous portion of the bone.

Mouse #1 had 2 submuscular beads implanted lateral to the tibial tuberosity approximately, 1 cm distal to the tibial plateau, and 1 submuscular bead placed under the quadriceps immediately lateral to the femur.

Mouse #2 had only 1 submuscular bead placed in a tibial location similar to mouse #1 and 1 intraosseous bead was inserted into the cortical bone of the femur from the lateral side. This procedure was performed by boring a small hole into the bone using a 25 gauge hypodermic needle (see Figure 2-4) and placing the bead into the hole.

The beads were sterilized using 70% ethanol solution prior to implantation. After the implantation, the incision was closed using dissolvable sutures and the mice were given a one-month recovery period.



**Figure 2-4** Incision into the femur using a 25 gauge hypodermic needle.

### 2.2.6 In vivo vibration amplitude measurement based on motion blur

A mouse was placed in the reference-bead cage, which was mounted on the vibration platform, and then set of 8 static (no vibration) x-ray images was acquired. The  $y$ -to- $x$  SD ratio was calculated for each of the 8 static images and those values were averaged.

The mouse vibration platform was then vibrated at a frequency of 30 Hz, under 0.43  $g$  ( $4.2 \text{ m/s}^2$ ) of acceleration, and with an amplitude of 118  $\mu\text{m}$ , and a second set of 8 dynamic x-ray images was acquired. Again, the  $y$ -to- $x$  SD ratio was calculated for each of the 8 dynamic images and the ratios values were averaged.

The mice were fully conscious during the WBV process because we required our data to be gathered under normal weight-bearing conditions – no drug or muscle relaxant was administered, which may have affected biomechanics or *in vivo* vibration transmission. As result, some of the acquired images suffered from additional blurring caused by the random movement of the mouse. However, it was relatively easy to determine whether an image was affected by mouse motion by checking to see that no significant Gaussian broadening along the  $x$  axis was observed in the reference bead profiles. Images with obvious  $x$  axis motion during imaging were rejected. A set of 8 images for each static and dynamic case are used in our analysis.

Lastly, the intensity profile fitting model *in vivo* is different than the standard 2-D Gaussian from equation (4). *In vivo*, the beads are in close proximity to the bone. Thus, the background pixel intensity values could have abrupt variations at the location of the bone interface. To account for these background intensity trends, a cubic term was added to the last term in equation (4). We must also consider the possibility of a small tilt ( $\theta$ ) in the axis of measured vibration, relative to the direction of the applied vibration, due to the propagation of the vibration *in vivo*. Therefore, for our analysis, we used the following analytical 2-D Gaussian model for fitting the intensity profile *in vivo*, which takes both abrupt background intensity fluctuation and the non-normal vibrational axis into account.

$$f(x, y) = A \cdot \exp \left[ - \left( \frac{((x - x_0) \cos(\theta) - (y - y_0) \sin(\theta))^2}{2\sigma_x^2} + \frac{((y - y_0) \sin(\theta) + (x - x_0) \cos(\theta))^2}{2\sigma_y^2} \right) \right] + ax^3 + bx^2 + cx + dy^3 + ey^2 + fy \quad (5)$$

$$+ k$$

where the parameters  $A$ ,  $x_0$ ,  $y_0$ ,  $k$ ,  $\sigma_x$ , and  $\sigma_y$  are previously defined from equation (4). And  $a$ ,  $b$ ,  $c$ ,  $d$ ,  $e$ , and  $f$  are constants. The cubic terms at the end of the equation (5) represents potential gradient in the image as result of different biological features on the x-ray image.

## 2.3 Results and Discussion

### 2.3.1 The effect of harmonic vibration on beads

Single x-ray images of a 280  $\mu\text{m}$  diameter reference-bead attached to the cage wall are shown in Figure 2-5 for the static case and several vibrational amplitudes: (a) 0  $\mu\text{m}$ ; (b) 78  $\mu\text{m}$ ; (c) 118  $\mu\text{m}$ ; (d) 157  $\mu\text{m}$ ; (e) 196  $\mu\text{m}$ ; (f) 237  $\mu\text{m}$ ; and (g) 277  $\mu\text{m}$ . Figure 2-6 shows plots of the intensity profiles along y-axis (parallel to the axis of vibration) of the bead through its centroid over a range of amplitudes.

As the vibrational amplitude increases, the residency time of a bead in any given pixel decreases resulting in blurring, decrease in contrast, and a higher local minimum in pixel intensity.

As the peak-to-peak amplitude approaches and exceeds the diameter of the bead, the intensity profile begins to assume a bimodal distribution due to the nature of simple harmonic motion. In particular, at the two extreme points of displacement, the instantaneous velocity is zero. Also, at the mid position between the extremes, the bead has the fastest instantaneous velocity. Therefore, in terms of a probability distribution, it is more likely for the CCD to register the bead at the two extreme points, than at the mid position. This is clearly demonstrated by the pixel intensity profile. This behavior can also be predicted from the harmonic motion induced PSF in (equation (3)) where, as  $x$  approaches  $\pm L$ , the function approaches infinity. Therefore, as long as the peak-to-peak vibration amplitude is below the diameter of the bead (280  $\mu\text{m}$ ), we can safely approximate the intensity profile with a Gaussian function.

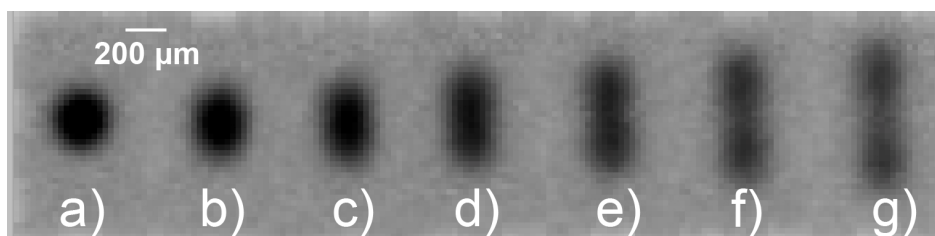


**Figure 2-5** Images of a single reference-bead used to calculate the  $y$ -to- $x$  SD ratio at different vibrational amplitudes for calibration: (a) 0  $\mu\text{m}$ ; (b) 78  $\mu\text{m}$ ; (c) 118  $\mu\text{m}$ ; (d) 157  $\mu\text{m}$ ; (e) 196  $\mu\text{m}$ ; (f) 237  $\mu\text{m}$ ; and (g) 277  $\mu\text{m}$ .

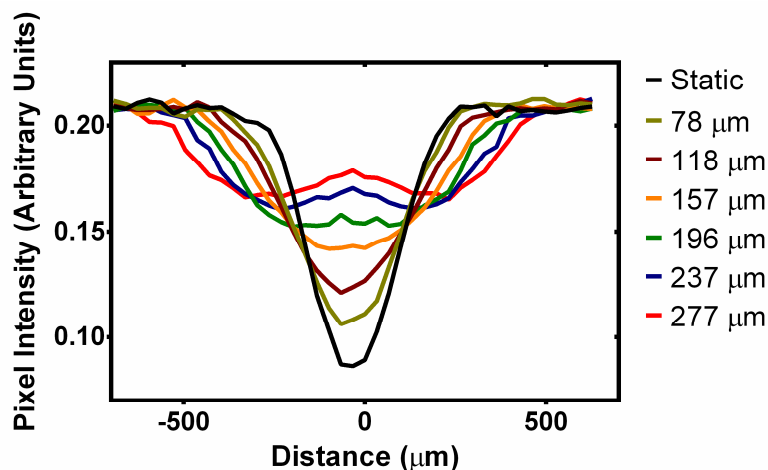


**Figure 2-6** Line profiles across the reference-bead parallel to the  $y$ -axis (direction of simple-harmonic motion) for a range of vibration amplitudes.

### 2.3.2 Vibration amplitude measurement and calibration

We have shown that we can approximate a motion-blurred bead profile with a Gaussian function as long as the peak-to-peak vibration amplitude is less than the diameter of the bead. The intensity profile of the bead is fitted to equation (4). The calculated SD in the  $y$ -direction (parallel to the direction of vibration) is then divided by the calculated SD in the  $x$ -direction (perpendicular to the direction of vibration). Figure 2-7 shows a plot of the reference-bead  $y$ -to- $x$  SD ratios as a function of vibration amplitude used as the calibration curve for our *in vivo* measurements.

Non-linear regression analysis revealed a quadratic relationship ( $R^2 = 0.9994$ ) between the  $y$ -to- $x$  SD ratio and the vibration amplitude, which strongly agrees with the analytical expression for the relationship.

To measure vibration amplitude *in vivo*, one has to acquire images of the vibrating beads, measure the SD ratio in both the  $x$  and  $y$  directions, calculate the  $y$ -to- $x$  SD ratio, and then look up the ratio on the characteristic curve of  $y$ -to- $x$  SD ratio vs. vibration amplitude to determine vibration amplitude. In this manner, harmonic vibration amplitude can be



quantified by exploiting motion-blur that manifests as a selective broadening of the 2-D Gaussian profile of the bead in the direction of the applied vibration.

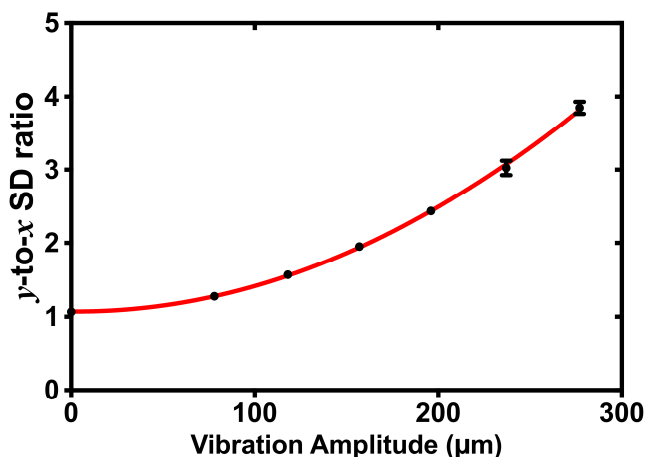


**Figure 2-7** The characteristic curve of  $y$ -to- $x$  SD ratios for reference-bead motion-blur at each vibration amplitude (error bars are standard deviation of the mean) used for calibration of the vibration system.

It is worth noting that the last two data points in the plot have a higher margin of error than the rest of the curve. This is due to the profile of the beads deviating from a Gaussian distribution toward a bimodal one as the peak-to-peak vibration approaches and exceeds the diameter of the bead.

A surprising observation from our data for the static scenario (zero amplitude) was that the  $y$ -to- $x$  SD ratio was not exactly equal to 1. The relative spatial resolution in the horizontal ( $x$ ) and vertical ( $y$ ) directions of the detector was investigated using a line-pair phantom (Nuclear Associates, Carle Place, N.Y.). It was observed visually that the spatial resolution along  $x$  is slightly better than along  $y$ . This small, but detectable, additional blur along the  $y$ -axis on the image revealed that the x-ray focal spot had a slightly asymmetrical shape, causing asymmetric resolution. Regardless of the absolute value of the  $y$ -to- $x$  SD ratio, this technique is able to accurately and reliably quantify vibration amplitude.

It is clear from the characteristic curve of  $y$ -to- $x$  SD ratios that our technique is able to reliably quantify vibration amplitude in the optimal range, between 100  $\mu\text{m}$  and 200  $\mu\text{m}$ ,

with a very small margin of error, provided that the period of vibration is much shorter than the exposure time of the CCD (*i.e.* approximately 630 ms).

### 2.3.3 In vivo vibration amplitude measurement

The weight of mice 2 weeks post-surgery were 23 g and 23 g for mouse #1 and mouse #2 respectively. The mice were in good health even though their overall weight dropped by 2 g, which is expected post-surgery. Currently, the biocompatibility of tungsten carbide is not very well documented in the literature. However, we have observed no obvious adverse effects in the mice during this study.

Figure 2-8 (a) and (b) shows an example of 2-D Gaussian fit of the bead *in vivo* using equation (5). Note that the close proximity of the bone contributed to the cubic behavior of the background pixel, which was taken into account in equation (5). Figure 2-9 (a) and (b) show static images of the tungsten-carbide beads implanted in the mice (circled in white). All other beads are the reference beads that are attached to the acrylic cage to monitor the applied vibration. Figure 2-9 (c) and (d) show images of the two mice during WBV at 118  $\mu\text{m}$  vibration amplitude. Note the circular appearance of all of the static beads, Figure 2-9 (a) and (b), and the vertical blurring of the beads in the dynamic WBV cases, Figure 2-9 (c) and (d) which is exploited to measure the vibrational amplitude.

The derived *y-to-x* SD ratios for each of the 4 cases are plotted in Figure 2-10. A commercially available statistics package (“Prism”, GraphPad Software, La Jolla, CA) was used to perform a one-way, non-parametric ANOVA on the data set from each of the 8 acquired images. Statistical significance is defined as  $p \leq 0.05$ . No statistically significant difference in the *y-to-x* SD ratios was found between any reference beads, so their values were averaged to provide greater statistical power.

In the static case for mouse #1 (Figure 2-10 (a)), none of the *y-to-x* SD ratios for the beads at the proximal tibia, distal tibia, and femur were statistically significantly different from the reference beads (Adjusted  $p > 0.999$ ,  $p > 0.999$ ,  $p = 0.473$  respectively). This indicates that the animal was in fact motionless during imaging.

The same result was observed in mouse #2 (Figure 2-10 (b)), in which there were no statistically significant differences between the  $y$ -to- $x$  SD ratios for the proximal tibia and femur beads in comparison to the reference beads (Adjusted  $p = 0.873$  and  $p = 0.644$  respectively).

In the dynamic WBV case for mouse #1 (Figure 2-10 (a)), we observed no statistically significant difference in the  $y$ -to- $x$  SD ratios between the proximal tibia and distal tibia in comparison to the moving reference beads ( $p = 0.485$  and  $p > 0.999$  respectively). However, the  $y$ -to- $x$  SD ratio for the femoral bead was statistically significantly different from that of the moving reference beads ( $p = 0.007$ ).

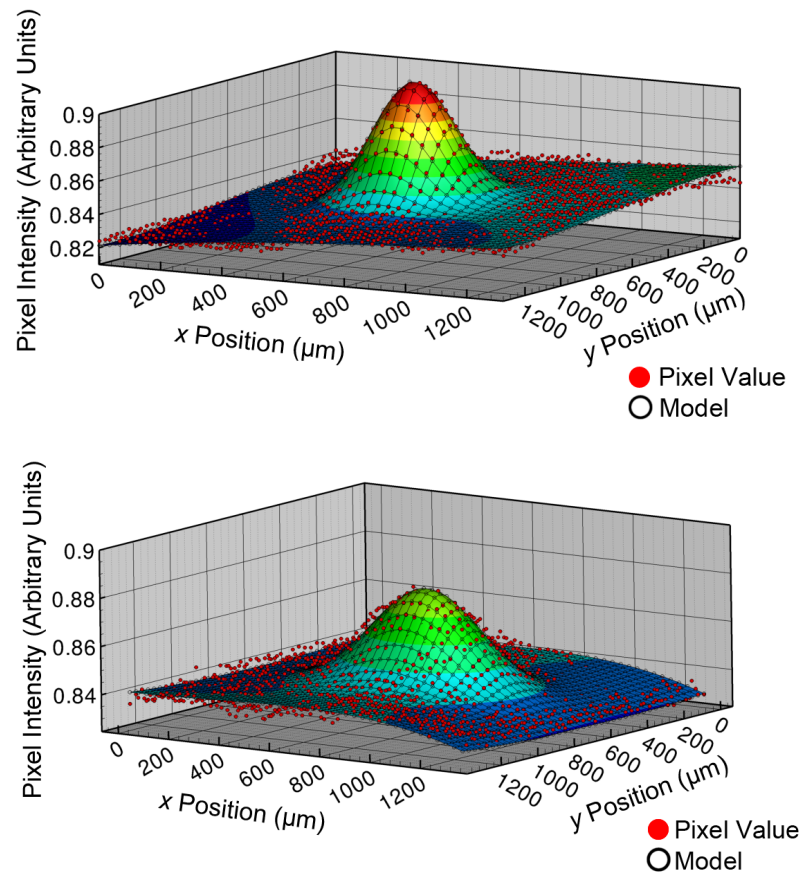


**Figure 2-8** Examples of fitting of a 2-D Gaussian surface to the *in vivo* beads using (5) in order to obtain SD. Note the cubic behavior of the background pixel in both plots. This was due to the close proximity of the bead to the bone. (a) Shows the static case, where there is no vibration. (b) Shows the dynamic case, where vibration is set at 0.43 g at 118 μm amplitude.

Similarly, in the dynamic WBV case for mouse #2 (Figure 2-10 (b)), no statistically significant difference was observed in the  $y$ -to- $x$  SD ratios for the tibia and the reference beads ( $p = 0.470$ ). However, the  $y$ -to- $x$  SD ratio for the femoral bead was statistically significantly different from that of the reference beads ( $p = 0.011$ ).

The  $y$ -to- $x$  SD ratios obtained from the WBV cases are then translated into vibration amplitude via the characteristic curve from Figure 2-7. The averaged vibration amplitudes measured from the images in each limb region are listed in Tables 2-2 and 2-3 for mouse #1 and mouse #2 respectively.

The measured vibration amplitudes from the reference beads of both mice are in good agreement with the input amplitude of the vibration platform, which is  $118 \mu\text{m}$ . As shown from our statistical test, the beads that were implanted in the femur in both mice vibrate at significantly different amplitude than all the other beads. In terms of the amplitude, this suggests that the femur in mouse #1 was experiencing vibration amplitude of  $99 \pm 7 \mu\text{m}$ , and  $102 \pm 11 \mu\text{m}$  for mouse #2.

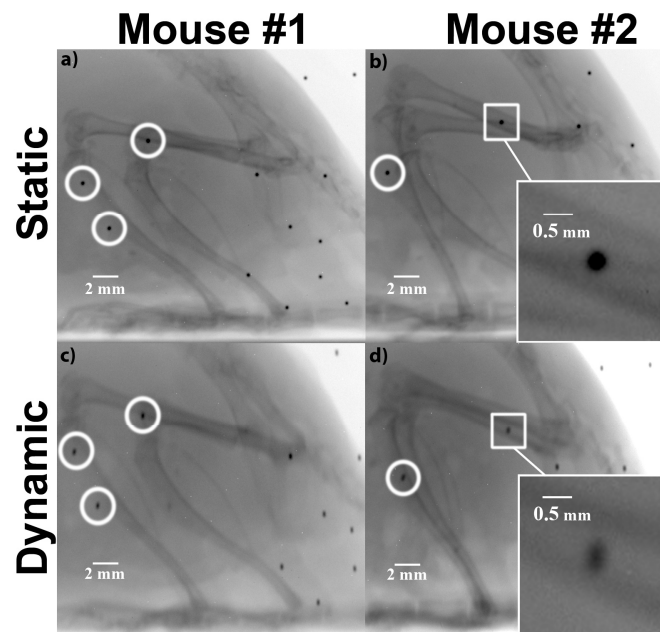


**Figure 2-9** *In vivo* images of implanted beads in mice, under both static conditions and while undergoing whole-body vibration: The bone-implanted beads are outlined in white circles. (a) Static x-ray image of mouse #1 (static conditions); (b) Static x-ray image of mouse #2 (static conditions); (c) WBV x-ray image of mouse #1 at vibration amplitude  $118 \mu\text{m}$ ; (d) WBV x-ray image of mouse #2 at vibration amplitude  $118 \mu\text{m}$ .

Knowing the vibration amplitude, we can further infer the peak-acceleration at those locations, assuming that the vibration frequency remains unchanged *in vivo*. The peak-acceleration can be obtained using equation (1). Therefore, at the femur of mouse #1 and mouse #2, the peak-acceleration is 0.37 g and 0.36 g respectively. In comparison to the input magnitude, which is 0.43 g, these are about 13% reduction in vibration magnitude.

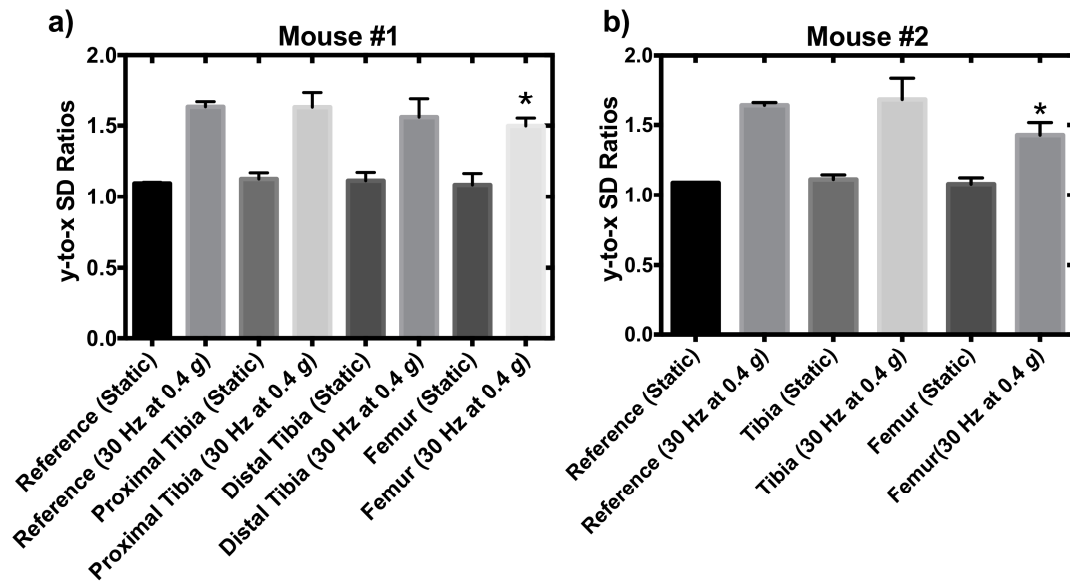


**Figure 2-10** (a) y-to-x SD ratios for mouse #1 with no vibration (static) and with vibration (dynamic). (b) y-to-x SD ratios for mouse #2 with no vibration (static) and with vibration (dynamic). Asterisk denotes statistical significance  $p \leq 0.05$  as compared to the reference bead in the dynamic case in both (a) and (b).

It is also interesting to observe there is no significant vibration reduction at the tibia. We speculate this was caused by the fact that tibia is in close contact with the vibration platform. Lastly, from the measured amplitude at the femur region of both mice, there is no difference between the bead physically implanted in the bone and the bead that is inserted under the muscle group right above the bone. Both surgical procedures yielded similar values. In terms of the surgical implantation technique, both implantation methods were relatively easy to perform and they were non-invasive in the sense that it caused any post-operative complication to the animal. However, in future study, we would use the intraosseous technique. This ensures that the bead indeed anchors firmly in the bone.

The high margin of error in some of the measured amplitudes is due to the confounding effects of background image features, such as bone, and the mathematical model used to fit the bead's intensity profile. However, our model is still robust enough to provide consistent measurement, providing that we have sufficient image data.

**Table 2-2** Vibration amplitude measured at each implanted region from mouse #1 based on SD ratios

	Amplitude ( $\mu\text{m}$ )	Standard Deviation ( $\mu\text{m}$ )
Reference Bead	121	4
Distal Tibia	110	12
Proximal Tibia	112	16
Femur	106	7

**Table 2-3** Vibration amplitude measured at each implanted region from mouse #2 based on SD ratios

	Amplitude ( $\mu\text{m}$ )	Standard Deviation ( $\mu\text{m}$ )
Reference Bead	122	2
Proximal Tibia	126	12
Femur	99	11

Although we have shown that our mouse cage is capable of keeping the mouse still during imaging, the cage still lacks a mechanism that prevents the mouse from turning within the enclosure. As result, at times it could take up to 2 hours to acquire a set of acceptable images per mouse. This issue can be addressed in the future by acclimatizing the animal with the cage and vibration protocol well before the experiment. One of the other limitations with our imaging system is the x-ray source. Specifically, the x-ray source isn't capable of acquiring multiple images within a short span of time before the x-ray tube overheats. This factor also contributes to the additional experiment time, which leads to a more agitated animal.

## 2.4 Conclusion

We have demonstrated a simple, reliable, and accurate imaging technique that exploits harmonic motion blur of fiducial markers to measure the transmission of whole-body vibration in small animals, provided one can consistently model the blurring of the bead, and correlate that with the vibration amplitude. This method can potentially be applied to

human subjects who already have metallic markers implanted in the bone, such as the case of radiostereometric analysis. This would eliminate the need for bone-attached accelerometers. Our future direction involves using this technique to assess vibration transmission for a range of amplitudes, magnitudes, and frequencies in mice.

## References

- (1) Rubin, C., Judex, S. & Qin, Y. X. Low-level mechanical signals and their potential as a non-pharmacological intervention for osteoporosis. *Age Ageing* **35**, 32-36, (2006).
- (2) Eisman, J. A. Good, good, good... good vibrations: the best option for better bones? *Lancet* **358**, 1924-1925, (2001).
- (3) Wolff, J. *Das Gesetz der Transformation der Knochen (The Law of Bone Remodelling)*. (Berlin: Verlag von August Hirschwald, 1892).
- (4) LeBlanc, A. *et al.* Bone mineral and lean tissue loss after long duration space flight. *Journal of musculoskeletal & neuronal interactions* **1**, 157-160, (2000).
- (5) Verschueren, S. M. P. *et al.* Effect of 6-month whole body vibration training on hip density, muscle strength, and postural control in postmenopausal women: A randomized controlled pilot study. *J Bone Miner Res* **19**, 352-359, (2004).
- (6) Gilsanz, V. *et al.* Low-level, high-frequency mechanical signals enhance musculoskeletal development of young women with low BMD. *J Bone Miner Res* **21**, 1464-1474, (2006).
- (7) LA, G.-T., MJ, G.-B., M, D. & JM., G.-A. Influence of the frequency of the external mechanical stimulus on bone healing: A computational study. *Medical Engineering and Physics* **32**, 363-371, (2010).
- (8) Delecluse, C., Roelants, M. & Verschueren, S. Strength increase after whole-body vibration compared with resistance training. *Med. Sci. Sports Exerc.* **35**, 1033-1041, (2003).
- (9) Rubin, C. *et al.* Prevention of postmenopausal bone loss by a low-magnitude, high-frequency mechanical stimuli: A clinical trial assessing compliance, efficacy, and safety. *J Bone Miner Res* **19**, 343-351, (2004).
- (10) Chen, B., Li, Y., Xie, D. & Yang, X. Low-magnitude high-frequency loading via whole body vibration enhances bone-implant osseointegration in ovariectomized rats. *Journal of Orthopaedic Research* **30**, 733-739, (2012).
- (11) Judex, S., Lei, X., Han, D. & Rubin, C. Low-magnitude mechanical signals that stimulate bone formation in the ovariectomized rat are dependent on the applied frequency but not on the strain magnitude. *J. Biomech.* **40**, 1333-1339, (2007).
- (12) Renshi, M. *et al.* High-frequency and low-magnitude whole body vibration with rest days is more effective in improving skeletal micro-morphology and



- biomechanical properties in ovariectomised rodents. *Hip International* **22**, 218-226, (2012).
- (13) Ogawa, T. *et al.* Influence of whole-body vibration time on peri-implant bone healing: a histomorphometrical animal study. *Journal of clinical periodontology* **38**, 180-185, (2011).
- (14) Wirth, F. *et al.* Whole-body vibration improves functional recovery in spinal cord injured rats. *Journal of neurotrauma* **30**, 453-468, (2013).
- (15) Behrens, V. *et al.* Vibration Syndrome in Chipping and Grinding Workers. *Journal of Occupational and Environmental Medicine* **26**, 765-788, (1984).
- (16) Bovenzi, M. Exposure-response relationship in the hand-arm vibration syndrome: an overview of current epidemiology research. *International Archives of Occupational and Environmental Health* **71**, 509-519, (1998).
- (17) Starck, J., Jussi, P. & Ilmari, P. Physical Characteristics of Vibration in Relation to Vibration-Induced White Finger. *American Industrial Hygiene Association Journal* **51**, 179-184, (1990).
- (18) Crewther, B., Cronin, J. & Keogh, J. Gravitational forces and whole body vibration: implications for prescription of vibratory stimulation. *Phys. Ther. Sport* **5**, 37-43, (2004).
- (19) Kiiski, J., Heinonen, A., Jaervinen, T. L., Kannus, P. & Sievanen, H. Transmission of vertical whole body vibration to the human body. *J Bone Miner Res* **23**, 1318-1325, (2008).
- (20) Pel, J. J. M. *et al.* Platform accelerations of three different whole-body vibration devices and the transmission of vertical vibrations to the lower limbs. *Med. Eng. Phys.* **31**, 937-944, (2009).
- (21) Nokes, L., Fairclough, J. A., Mintowt-Czyz, W. J., Mackie, I. & Williams, J. Vibration analysis of human tibia: the effect of soft tissue on the output from skin-mounted accelerometers. *Journal of biomedical engineering* **6**, 223-226, (1984).
- (22) Ziegert, J. C. & Lewis, J. L. The Effect of Soft Tissue on Measurements of Vibrational Bone Motion by Skin-Mounted Accelerometers. *Journal of Biomechanical Engineering* **101**, 218-220, (1979).
- (23) Rubin, C. *et al.* Transmissibility of 15-hertz to 35-hertz vibrations to the human hip and lumbar spine: determining the physiologic feasibility of delivering low-level anabolic mechanical stimuli to skeletal regions at greatest risk of fracture because of osteoporosis. *Spine* **28**, 2621-2627, (2003).
- (24) Holguin, N., Uzer, G., Chiang, F. P., Rubin, C. & Judex, S. Brief daily exposure to low-intensity vibration mitigates the degradation of the intervertebral disc in a

frequency-specific manner. *Journal of Applied Physiology* **111**, 1846-1853, (2011).

- (25) Pollmann, S. I., Norley, C. J. D., Yuan, X. H. & Holdsworth, D. W. in *Medical Imaging 2012: Physics of Medical Imaging* Vol. 8313 *Proceedings of SPIE* (Spie-Int Soc Optical Engineering, 2012).
- (26) Griffin, M. J. *Handbook of human vibration*. (Academic Press, 1990).
- (27) Hadar, O., Dror, I. & Kopeika, N. S. Image-Resolution Limits Resulting from Mechanical Vibrations .4. Real-Time Numerical-Calculation of Optical Transfer-Functions and Experimental-Verification. *Opt. Eng.* **33**, 566-578, (1994).

## Chapter 3

*In preparation for submission to the journal of Bone and Mineral Research*

### 3 Transmission of vertical whole-body vibration in mice

#### 3.1 Introduction

As describe in Chapter 1, there is currently great interest in the biological effects of applying mechanical stimuli, such as whole-body vibration (WBV), to the bones of humans and animals which results in increased BMD (bone mineral density) according to Wolff's law.<sup>1</sup> It has been proposed that this effect has the potential to be employed therapeutically to reverse osteoporosis and strengthen bones.<sup>2-5</sup> Current research suggests that high frequency (10 – 100 Hz), low magnitude vibration ( $< 1 g$ , where  $g$  is the acceleration due to the Earth's gravity,  $9.8 \text{ m/s}^2$ ), and relatively short duration ( $< 30$  minutes) exposure is most effective in anabolic bone synthesis in the skeletal system in both humans and animals.<sup>6-11</sup> In contrast, high magnitude ( $>> 1 g$ ) vibration and prolonged exposure can be harmful.<sup>12,13</sup>

The transmission of vibration in humans is typically measured at the skin level by affixing an accelerometer onto the skin at the site of interest.<sup>14-16</sup> However, studies have shown skin-mounted accelerometers do not accurately reflect the actual magnitude of vibration at the skeletal level.<sup>17-20</sup> This is due to the attenuation and damping caused by the soft tissue surrounding the bone. Fortunately, in human subjects this problem can be easily addressed, as it is relatively simple to attach accelerometers directly onto the bone through the use of such devices as a Kirschner wire.<sup>21</sup>

Small animals, such mice, are frequently used in musculoskeletal research due to their short life span, small size, and their similarity to humans in skeletal response to WBV. Inertia-based sensors that attach to animals would need to be proportionally small in order to not influence the measurement of vibration. Unfortunately, no implantable accelerometers of sufficiently small size and mass currently exist for mice or other small animals.

Perhaps, the biggest difference between human and animal subjects is that there is a greater experimental control factor in humans in terms of the ability to remain motionless. Thus, it is common practice to anesthetize the animal during the experiment, which prevents it from moving around in its local environment. Thus, the animals are usually laying in a prone position and not standing in a physiologically-realistic stance.<sup>22</sup> In the case of vertical vibration transmission, this unconscious posture causes diminished loading of the limbs compared to a conscious and standing posture.

An alternative method for measuring vibration transmission, that avoids implantable accelerometers, is known as the constrained tibial vibration (CVT) technique, from Christiansen *et al.*<sup>23</sup> But, as the name implies, this method is limited to the tibial region only. The response and interaction to the applied vibration, from adjacent structures – femur, tibia, and fibula combined as a whole – is ignored. Therefore, there is currently a lack of understanding of the vibration propagation at different skeletal levels in a rodent model under different vibration conditions, as well as how the animal's posture could affect the transmission.

In this chapter transmission of vertical vibration at the tibial and the femoral region in mice is characterized using the novel imaging technique described in Chapter 2, for vibrational frequencies between 15 – 40 Hz and peak-acceleration (vibration magnitude) between 0.09 – 0.87 g. These ranges of vibration parameters are used in animal whole-body vibration because they have been previously reported to promote bone growth.<sup>24,25</sup> Moreover, the animals under study were kept fully conscious so that the limbs would be under normal weight-bearing condition during the therapy.

## 3.2 Material and Methods

All procedures were approved by the University of Western Ontario Animal Use Subcommittee and were conducted in accordance with guidelines set out by the Canadian Council on Animal Care. A total of six C57BL/6J male mice were used in the experiment. The mice were 13 weeks old, all male, and weighed  $27 \pm 1$  g.

### 3.2.1 Fiducial Markers Implantation

From Chapter 2, we presented a novel technique of quantifying vibration *in vivo* based on motion-blurred fiducial markers – 280  $\mu\text{m}$  diameter, tungsten-carbide beads (New England Miniature Ball Company, Norfolk, CT). The mice were given prophylactic, pre-surgical antibiotics (Meloxicam, 0.01ml/kg, Boehringer Ingelheim Vetmedica Inc., St. Joseph, MO) to minimize the risk of infection. Bead-implantation surgery was carried out with the animals sedated using a 2% isoflurane anesthetic. The beads were sterilized using a 70% ethanol solution and implanted at the tibia crest and mid-diaphysis of the femur of the animal. A 25-gauge hypodermic needle was used to penetrate the cortical bone of the animal. The bead was then placed into the bone and the wound was closed with a suture. In total, the mice were given one month of recovery in order to allow the beads to have sufficient time for osteointegration.

### 3.2.2 Imaging System and Processing

A 2-D X-ray projection imaging was used to observe the fiducial markers *in vivo*. The x-ray source was a ceiling mounted x-ray unit (Proteus XR-a, GE Medical Systems, Milwaukee, WI, USA). An indirect x-ray imaging method was used where x-ray photons were passed through the subject, converted into visible-light photons using a scintillating material (Kodak, Min-R2 2000 screen, Rochester, NY), and then an image of the scintillator was captured by a CCD camera (Cascade 1K, Photometrics, Tucson, AZ), which was controlled via  $\mu\text{Manager}^{26}$  software. The energy of the x-ray was set to 80kV<sub>p</sub> at 200 mA, and 0.63 ms exposure for all of the experiments. The imaging system was integrated with the whole-body vibration platform as shown in Figure 3-1. Image post-processing was done using MATLAB environment (MathWorks, Natick, MA).

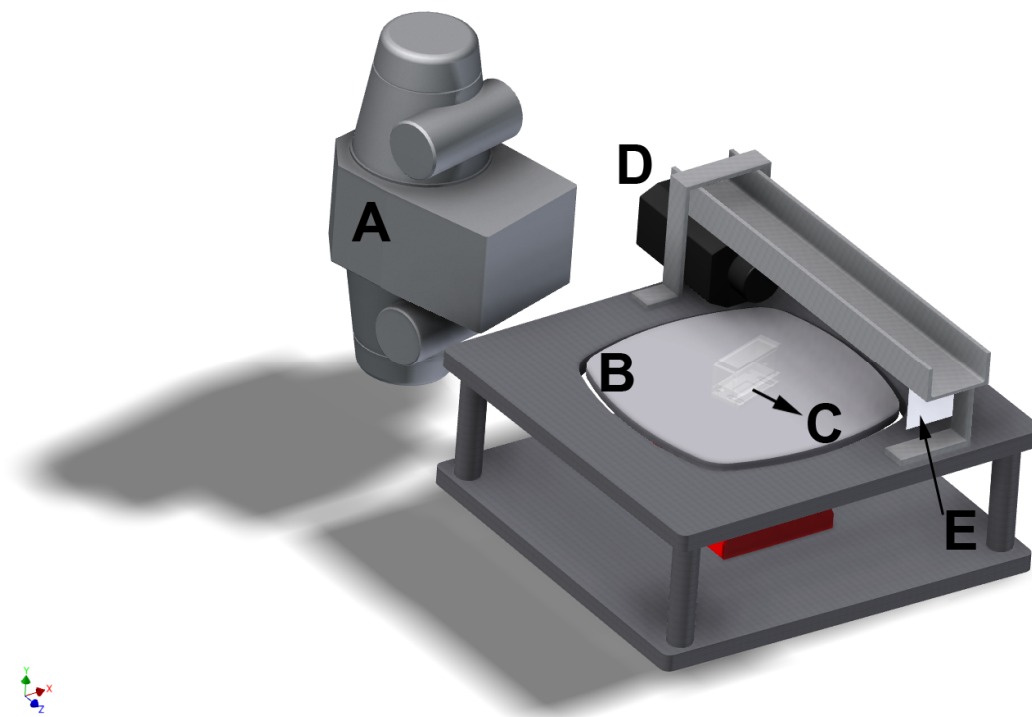


**Figure 3-1** The digital imaging system consists of an x-ray source (A), vibration platform (B), mouse cage (C), scintillating screen (D), and a CCD camera (E). The image system is integrated with a vibration platform so that *in vivo* vibration can be quantified. The x-ray is imaged indirectly; first it is converted into visible photons, via a scintillating screen, which are then captured by a CCD camera.

### 3.2.3 Whole-body Vibration Platform and Mouse Cage

At the heart of the whole-body vibration platform is an electromagnetic shaker (Type V20, Signal Force, Data Physics Corp., San Jose, CA) capable of accurately producing vibration in the range of 10 – 100 Hz and 0 – 1 g. A waveform generator (Model 148A, WaveTek, AeroFlex, Plainview, NY) controlled the input waveform to the vibration platform. The signal from the waveform generator was amplified via a 100W power amplifier (Signal Force, Data Physics Corp., San Jose, CA) in order to drive the shaker. The frequency and the magnitude of the resultant vibration produced by the shaker were monitored by an accelerometer (Model 7500A1, Dytran Inc., Chatsworth, CA) firmly affixed to the vibration platform. The waveform generator input and accelerator output were recorded using an analog-to-digital recorder (ML750 PowerLab/4SP, ADInstruments Inc., Colorado Spring, CO).

The mouse remained non-sedated and conscious during the experiment, in order to maintain a natural posture and measured transmissibility of the bone – a sedated mouse would be laying in a prone position with no weight bearing on the limbs. The predisposition of mice to virtually-constant motion and “fidgeting” poses significant motion-related problems to the imaging process of a non-sedated animal. While physical restraint of the animal would affect the measured transmissibility, we found that by limiting the space in which the mouse is allowed to move minimizes its motion and allowed the acquisition of un-blurred images. Thus, a custom mouse cage (Figure 3-2), with inner dimensions 8.3 cm long x 4.0 cm wide x 3.5 cm high, and with two  $\frac{3}{4}$ ” ventilation holes, was fabricated from  $\frac{1}{4}$ ” thick acrylic. The box confines the animal so that it is unable to move laterally or longitudinally. The restraining box was magnetically attached to the vibration platform to allow its free orientation relative to the x-ray source without sacrificing good contact with the platform. Fiducial markers were glued on the side of the restraining box to function as reference beads, from which applied vibration amplitude could be measured and compared to the *in vivo* vibration amplitude of the bones.

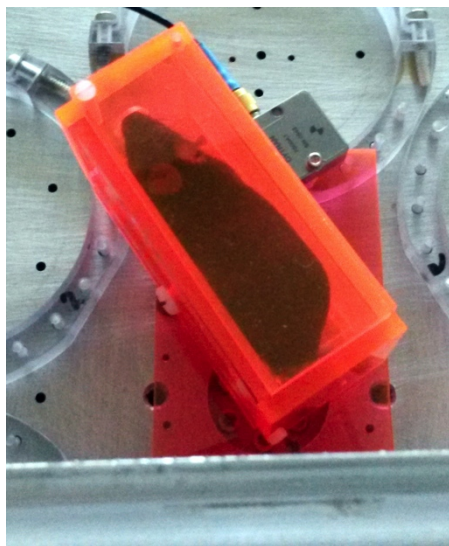


**Figure 3-2** To prevent the mouse from moving around during imaging, a cage is designed and built such that it limits the animal’s mobility.

### 3.2.4 Vibration Protocols

Table 1 lists the vibration frequencies and magnitude used in the experiment. The peak amplitudes of vibration were derived according to Griffin<sup>27</sup>. The mice were first placed in the restraining box, and allowed to acclimatize to the confined environment with vibration of 25 Hz at 0.28 *g* for 10 minutes. After which, the vibration protocol was initiated from 15 Hz, at the lowest magnitude and progressively increased. A set of 8 x-ray images were obtained for each vibration condition, per mouse.

### 3.2.5 Measurement of transmissibility and its dependence on vibration frequency

For each of the 8 images acquired at one set of vibrational parameters, the intensity profile of each reference bead and each implanted bead in the x-ray image was fitted to a 2-D Gaussian surface. Our previous study (Chapter 2) showed that there is a quadratic relationship between the broadening of the intensity profile, in the direction of motion, due to motion blur and the vibration amplitude. Therefore, this allows us to infer any vibration amplitude based on motion blur. The transmissibility was then calculated as the ratio of the measured *in vivo* vibration amplitude to the measured reference amplitude by taking the ratio between the two.

The amplitudes measured from the eight mice were averaged, categorized according to frequency, and plotted for each magnitude of the same frequency group. Lastly, averaging the transmissibility values over the entire peak-acceleration category of the same frequency group produced the dependence of transmissibility on vibration frequency plot.

### 3.2.6 Dependence of transmissibility and postures

Since the mouse was non-sedated, it could be in quite a variety of standing postures during imaging. We identified three possible scenarios: normal standing position (Figure 3-3a), crouch position (Figure 3-3b), and extended position (Figure 3-3c). Additionally, we defined the angle between the animal's tibia and femur as a parameter that could affect the transmissibility. This angle was measured from two imaginary lines (Figure 3-4): Line 1 was drawn from the distal tibia and extending longitudinally, passing through



the implanted bead; Line 2 was drawn from the proximal femur and extending longitudinally, passing through the implanted bead. This angle measurement was performed for all of the images in ImageJ.<sup>28</sup>

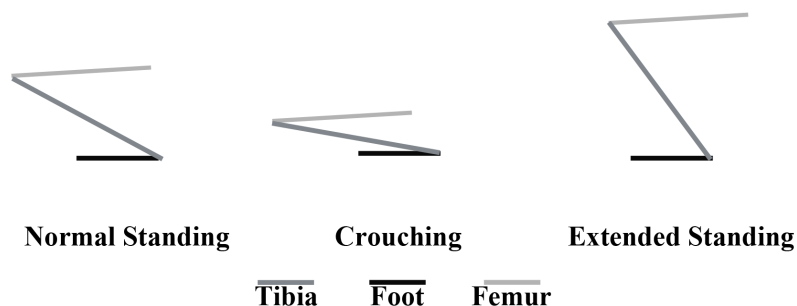


**Figure 3-3** The three possible animal postures during imaging are (a) normal standing position, (b) crouch position, and (c) extended leg position.

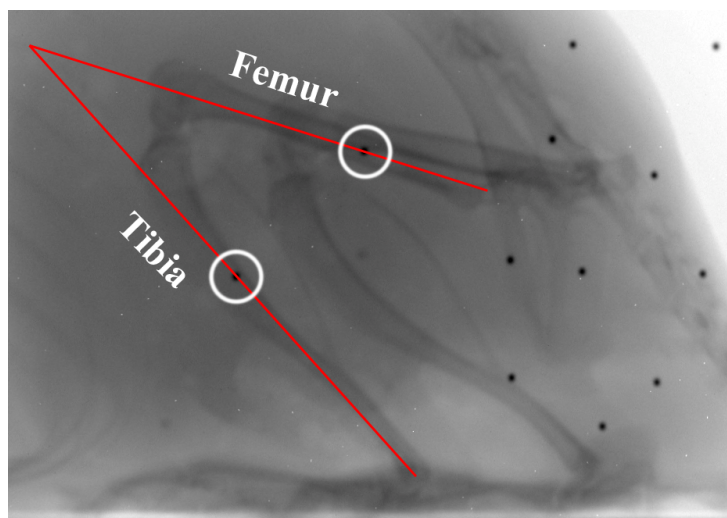


**Figure 3-4** The angle between the femoral and tibial bone is defined by the two imaginary lines drawn through the respective bones as shown. The implanted beads are circled. The femoral line starts at proximal femur and extends longitudinally, through the implanted bead. Similarly, the tibial line starts at the distal tibia and extends longitudinally, through the implanted bead. The angle between the two lines is then measured in ImageJ.

**Table 3-1** Vibration Protocols used in *in vivo* experiment

Frequency (Hz)	Magnitude (g)	Theoretical Amplitude ( $\mu\text{m}$ )
15	0.09	102
	0.14	157
	0.18	204
20	0.14	88
	0.21	132
	0.28	177
25	0.28	113
	0.36	141
	0.45	181
30	0.57	157
	0.64	177
	0.71	196
35	0.57	115
	0.64	130
	0.71	144
40	0.57	88
	0.64	99
	0.71	110
	0.85	132

### 3.2.7 Data Analysis

Statistical package, GraphPad Prism 6.0 (GraphPad Software, La Jolla, CA), was used for all of our statistical analyses. Repeated measure one-way ANOVA was used for the transmissibility analysis. Correlation was used to examine the relationship between postures and transmissibility. Statistical significance is defined as  $p \leq 0.05$ .

## 3.3 Results

The health of the mice was closely monitored by observing their weight for two weeks after surgery. No significance ( $p = 0.055$ ) was observed between the mice weight pre-implantation and 2 weeks post-implantation, which indicated good health. In addition, no side effects associated with the implantation of tungsten carbide material *in vivo* were observed during our study.

A typical data acquisition time was 30 minutes. This time is limited by the x-ray tube, which overheats after 30 min period. However, it is possible to complete one set of vibration magnitude per frequency per mouse within that time frame.

An x-ray image of one of the mice during WBV is shown in Figure 3-5. Note the elongate shape of the bead due to motion-blur. The implanted beads are highlighted, and the scattered beads on the right are the moving reference beads, affixed to the cage.

The measured *in vivo* vibration amplitudes for each magnitude at the same frequency group are plotted in Figure 3-6. It was observed that between 15 – 25 Hz, there was a significant increase in the *in vivo* vibration amplitude in the femur compared to the reference amplitude. At 15 Hz, at a magnitude of 0.14 g and 0.18 g, the *in vivo* vibration amplitude in the femur increased by 13% ( $p = 0.014$ ) and 11% ( $p = 0.016$ ) over the respective reference amplitudes. At 20 Hz, with magnitude of 0.21 g and 0.28 g, the *in vivo* vibration amplitude increased by 19% ( $p = 0.014$ ) and 20% ( $p = 0.001$ ) respectively over reference values. Lastly, at 25 Hz, with magnitude of 0.28 g and 0.36 g, the *in vivo* vibration amplitude increased by 26% ( $p = 0.010$ ) and 36% ( $p = 0.011$ ) over respective reference values. No significant changes were observed for the tibia at those frequency ranges. It is noteworthy that, at 30 Hz, there was a sudden decrease of 11% ( $p = 0.0175$ ) and 12% ( $p = 0.0422$ ) in the transmitted *in vivo* vibration amplitude in the tibia at the magnitude of 0.64 g and 0.71 g compared to reference values. No significant difference was observed in the femur at 30 Hz. Finally, no significant difference was observed between the reference amplitude and the measured *in vivo* amplitudes in tibia and femur in the 35 – 40 Hz range.

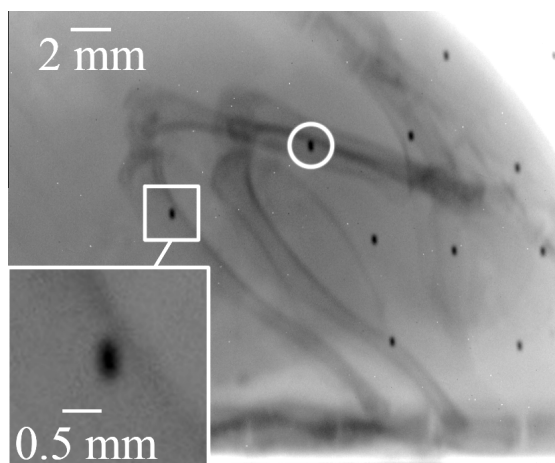


**Figure 3-5** An x-ray image of the animal in the restrainer. The implanted beads are highlighted. The scattered beads on the right are the reference beads, which are glued onto the restrainer. Note the elongation of the bead in the vertical direction due to motion blur.

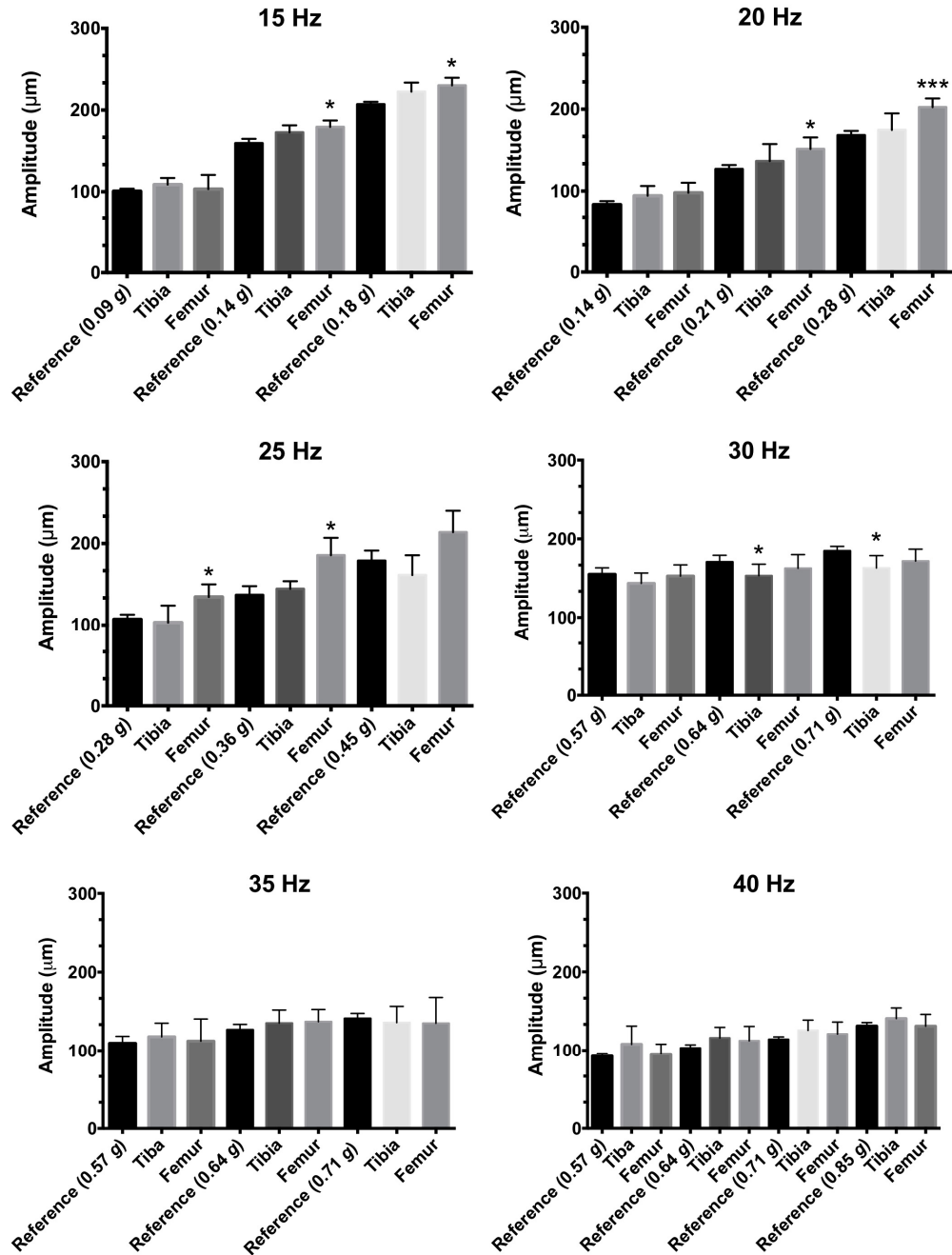


**Figure 3-6** The vibration amplitudes of each peak-acceleration category of the same vibration frequency group are plotted. An asterisk denotes statistical significance when compared to the corresponding reference amplitude at the same peak-acceleration and vibration frequency (\*  $p < 0.05$  and \*\*  $p < 0.001$ ).

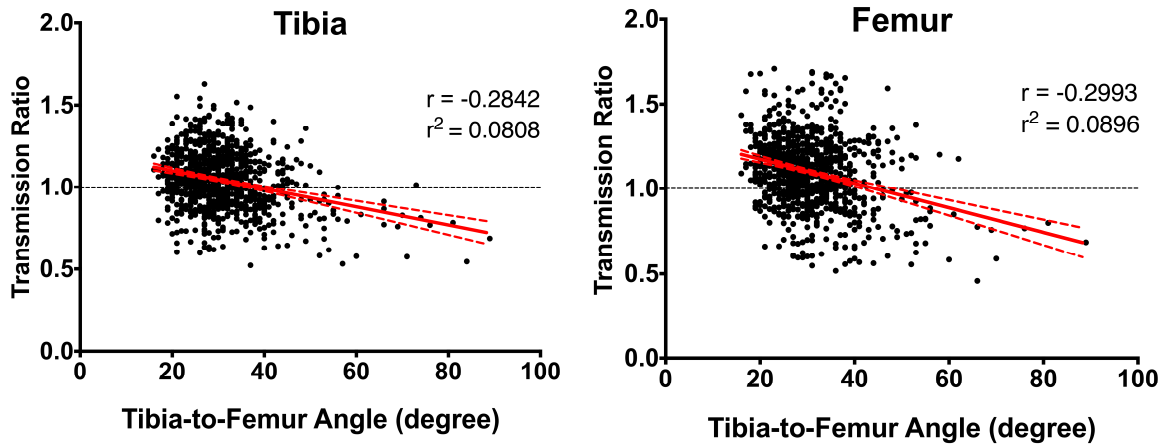


**Figure 3-7** The transmissibility values from all the data are plotted against their corresponding tibia-to-femur angle. The transmissibility and animal posture have negative correlation. In the tibia,  $r = -0.2842$ . And,  $r = -0.2993$  in the femur. This suggests that as the angle between the tibial bone and femoral bone decreases, the transmissibility increases.

Since the postures of the mice were not a controllable parameter, only a limited number of data points were available for the extended position and crouch position. Nevertheless, a weak negative correlation between the transmissibility and tibia-to-femur angle was observed in the tibia ( $r = -0.2842$ ) and the femur ( $r = -0.2993$ ) as shown in Figure 3-7. Note that majority of data points clusters in the tibia-to-femur angle range of 30 – 40 degrees, suggesting that these are the normal standing posture of the animal.

Figure 3-8a and 3-8b show the dependency of transmissibility on vibration frequency for tibia and femur respectively. It is clear that the transmissibility in the femur gradually increases from 15 Hz to a maximum at 25 Hz after which the transmissibility decreases towards 30 – 40 Hz. A different behavior was observed in the tibia where the transmissibility dips to a minimum at 30 Hz, but remains relatively constant at all other vibration frequencies.

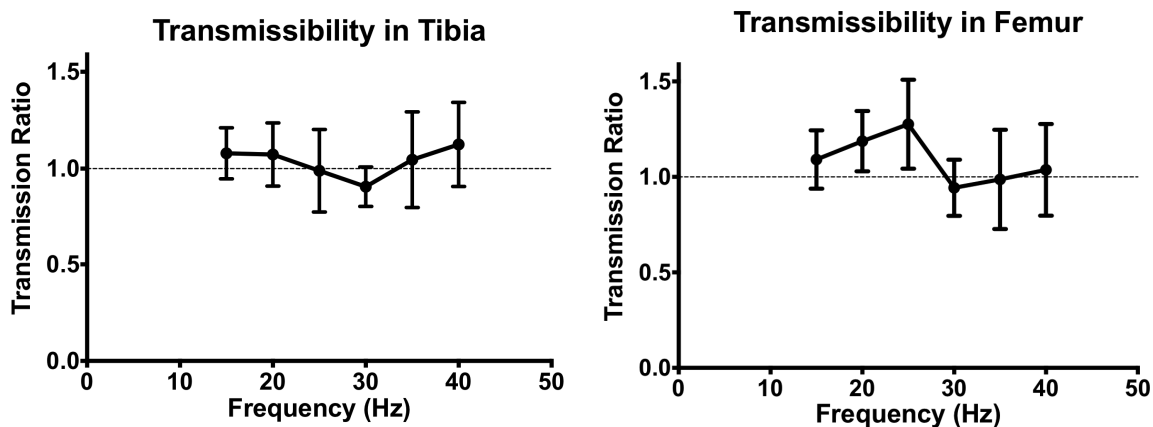


**Figure 3-8** The transmissibility from the entire peak-acceleration category of the same frequency group are averaged and plotted for each frequency group. The behavior of the transmissibility in the tibia across 15 – 40 Hz range and the behavior of the transmissibility in the femur across 15 – 40 Hz range are shown. Note the increasing transmissibility in the femur in the 15 – 25 Hz range.

### 3.4 Discussion

Our objective was to characterize the transmission of vertical, whole-body vibration in mice using our previously developed, novel, *in vivo*, skeletal-vibration quantification technique. Our results indicate that the transmissibility is frequency-dependent for both femur and tibia – a resonance was observed in the femur at 25 Hz, along with a small decrease in the transmissibility in both femur and tibia at 30 Hz. We have chosen to characterize the transmission of vertical vibration in mouse in the frequency range 15 – 40 Hz because that is the region most often explored in the literature.

There is currently virtually no *in vivo* information available in the literature with which we can compare our results. Previous studies have developed finite-element models (FEM) to analyze the natural frequency of isolated murine tibia and femurs. Nemani and Yokota<sup>29</sup> report a broad resonance (1<sup>st</sup> mode) of the femur near 23 Hz, which is in agreement with our observations (25 Hz) of the femur. They also reported an additional resonance at 33 Hz, which we did not observe – in fact, we saw a slight reduction in the transmissibility at 30 Hz. In the tibia, we observed no resonance in the 15 – 40 Hz frequency range, contrary to the previously reported FEM results and they reported no dip in the frequency response around 30 Hz. Factors which may explain some of these discrepancies are the gross size of the bones and related age and weight of the mice, non-

homogeneous nature of the bone, and the examination in the FEM study of the bones in isolation – unconnected to adjacent bones (tibia, femur, fibula, pelvis, feet) and other soft tissue, such as tendons and cartilage.

*Ex vivo* vibration experiments have been conducted in which vibration was localized to the isolated tibia and the femur. Kim *et al*<sup>30</sup> reported that the natural frequency resonance (1<sup>st</sup> mode) of the femur is in the range of 20.9 – 25.6 Hz. Once again, the resonance we observed from our *in vivo* experiment falls within this frequency range. Christiansen *et al*<sup>23</sup> characterized the transmissibility of the tibia over a much broader range than our study (20 – 150 Hz). Their observations of no resonances in transmissibility for the tibia in the 20 – 40 Hz range are consistent with ours, including the dip in frequency response at approximately 30 Hz.

A murine model is different from that of human in many ways (bone size, muscle mass, posture, *etc.*). Thus, a direct comparison between the transmissibility curves (Figure 3-8) obtained here with that of human is not appropriate. However, there are features that are common in mice WBV and human WBV, specifically, resonance (amplification) and damping. Rubin *et al.*, observed a resonance in the hip at frequencies less than 20 Hz using bone-mounted accelerometer.<sup>21</sup> Similarly, using a skin-mounted accelerometer, Juha *et al.* observed resonance in the ankle, knee and hip.<sup>14</sup> Damping effect was also observed in both studies, although it only occurred in the < 20 Hz region.

There have been several reports that the mechanical-signaling mechanism associated with bone formation is frequency-dependent, rather than strain-dependent.<sup>31-33</sup> This could be attributed to the fact that resonance occurs at a specific frequency, as we have shown. Therefore, if whole-body vibration is applied at the resonance frequency, then vibration magnitude can be relatively low, since it would be amplified *in vivo* by the effect of the resonance. Furthermore, because the tibia and femur have slightly different resonance frequencies, the potential exists to target the vibration to a specific bone<sup>34</sup>.

We also found that the transmissibility is dependent on the posture of the animal. When the animal is in a crouched position, more vibration is being transmitted to its body. But, when the animal extends its body in a standing posture, *i.e.*, when the angle between tibia

and the femur is greatest, less vibration is transmitted. Note also that our data has a wide distribution, suggesting biological variability between each mouse.

In human whole-body vibration, standing posture affects the vibration transmissibility.<sup>15,35</sup> Similarly, one would expect the transmissibility in mice to be posture dependent. But unlike human studies, we do not have control of the animals' posture during the experiments. Therefore, we can only indirectly infer the posture using the knee flexion angle from each image. As expected, posture and transmissibility are correlated, as shown in Figure 3-7. When the animal is in a crouch position, we observed more vibration being transmitted into the skeletal system because its belly is in contact with the vibration platform. Thus, the overall transmitted vibration is increased due to the increased contact area. The opposite occurs when the animal is in an extended "standing" position, i.e., the angle between the femur and tibia is much greater than 40 degrees. Here we speculate that the leg muscle is under greater tension, which lowers the transmitted vibration. The opposite is true in humans, where a stiffer muscle correlates to better transmission of vibration.<sup>35</sup> More research is needed to determine the dampening of vibration when the leg muscle is activated in mouse.

There are two limitations associated with this technique. First, the resolution of the imaging system limits the smallest vibration amplitude that can be resolved. In our current setup, the effective pixel size is 33  $\mu\text{m}/\text{pixel}$ . This limits our ability to characterize transmissibility beyond 40 Hz, as vibration amplitude is proportional to the inverse square of frequency, if acceleration is held constant.<sup>27</sup> For example, with a peak acceleration of 0.4  $g$  at 90 Hz, the vibration amplitude is only about 12  $\mu\text{m}$ . To obtain detectable vibration amplitude at that vibration frequency for our imaging system, we would need to increase the peak acceleration to at least 2  $g$  – a regime where the vibrational stimulation ceases to promote healthy bone growth and begins to be destructive. We have also observed in our studies that the mice are not likely to tolerate such high-amplitude stimuli while remaining stationary. Simply changing the optical lens of the CCD will change the resolution of the imaging system, but at a cost of decreased field of view. This is problematic because it limits the number of beads that can be captured in a single image.



The second limitation relates to the location of the implanted beads in the bone and surgical considerations. There is limited area on the tibia and the femur in which the beads can be implanted in order to ensure firm implantation and minimal damage to the bone. For instance, in order to implant the bead at the distal femur, there are tendons that need to be cut in order to gain access. This procedure would be too invasive, which means longer recovery, and uncertain surgical outcome. These factors limit our ability to implant multiple beads per bone, which is desirable for determining how the vibration varies at different location of the bone. One possible solution is to affix the bead onto the bone with epoxy bone cement to reduce the invasiveness of the procedure while retaining firm contact with the bone. It is noteworthy that no animals died from any surgical complications, nor did we observe any negative reaction to the tungsten carbide bead implantation six-months post-surgery. We found no reports in the literature of problems related to the biocompatibility of tungsten carbide, or any known long-term *in vivo* effects. Based on our experience, tungsten carbide beads are safe for *in vivo* implantation, and preoperative sterilization is recommended.

In summary, this study presents first ever *in vivo* vibration characterization of transmission through the murine femur and tibia in the frequency range from 15 Hz to 40 Hz. It was observed that the femoral bone has a resonance near 25 Hz and the tibia has a significant decrease in transmissibility at 30 Hz. Future work will explore vibration transmission at other anatomical locations in the animal, such as the spine or pelvis. Additionally, it will be informative to compare skeletal vibration and skin-level vibration in mice by affixing fiducial beads directly onto the skin.

## References

- (1) Wolff, J. *Das Gesetz der Transformation der Knochen (The Law of Bone Remodelling)*. (Berlin: Verlag von August Hirschwald, 1892).
- (2) Banu, J., Varela, E. & Fernandes, G. Alternative therapies for the prevention and treatment of osteoporosis. *Nutrition reviews* **70**, 22-40, (2012).
- (3) Rubin, C., Judex, S. & Qin, Y.-X. Low-level mechanical signals and their potential as a non-pharmacological intervention for osteoporosis. *Age Ageing* **35 Suppl 2**, ii32-36, (2006).
- (4) Rubin, C., Turner, A. S., Bain, S., Mallinckrodt, C. & McLeod, K. Anabolism. Low mechanical signals strengthen long bones. *Nature* **412**, 603-604, (2001).
- (5) Chan, M. E., Uzer, G. & Rubin, C. T. The potential benefits and inherent risks of vibration as a non-drug therapy for the prevention and treatment of osteoporosis. *Current osteoporosis reports* **11**, 36-44, (2013).
- (6) Chen, B., Li, Y., Xie, D. & Yang, X. Low-magnitude high-frequency loading via whole body vibration enhances bone-implant osseointegration in ovariectomized rats. *Journal of Orthopaedic Research* **30**, 733-739, (2012).
- (7) Tezval, M. *et al.* Improvement of femoral bone quality after low-magnitude, high-frequency mechanical stimulation in the ovariectomized rat as an osteopenia model. *Calcif Tissue Int* **88**, 33-40, (2011).
- (8) Gilsanz, V. *et al.* Low-level, high-frequency mechanical signals enhance musculoskeletal development of young women with low BMD. *J Bone Miner Res* **21**, 1464-1474, (2006).
- (9) Rubin, C. *et al.* Prevention of postmenopausal bone loss by a low-magnitude, high-frequency mechanical stimuli: A clinical trial assessing compliance, efficacy, and safety. *J Bone Miner Res* **19**, 343-351, (2004).
- (10) McCann, M. R. *et al.* Acute vibration induces transient expression of anabolic genes in the murine intervertebral disc. *Arthritis Rheum* **65**, 1853-1864, (2013).
- (11) Turner, S. *et al.* A randomized controlled trial of whole body vibration exposure on markers of bone turnover in postmenopausal women. *Journal of osteoporosis* **2011**, 710387, (2011).
- (12) Griffin, M. J. & Bovenzi, M. The diagnosis of disorders caused by hand-transmitted vibration: Southampton Workshop 2000. *International Archives of Occupational and Environmental Health* **75**, 1-5, (2002).

- (13) Bovenzi, M. Exposure-response relationship in the hand-arm vibration syndrome: an overview of current epidemiology research. *International Archives of Occupational and Environmental Health* **71**, 509-519, (1998).
- (14) Kiiski, J., Heinonen, A., Jaervinen, T. L., Kannus, P. & Sievanen, H. Transmission of vertical whole body vibration to the human body. *J Bone Miner Res* **23**, 1318-1325, (2008).
- (15) Crewther, B., Cronin, J. & Keogh, J. Gravitational forces and whole body vibration: implications for prescription of vibratory stimulation. *Phys. Ther. Sport* **5**, 37-43, (2004).
- (16) Morgado Ramírez, D. Z., Strike, S. & Lee, R. Y. W. Measurement of transmission of vibration through the human spine using skin-mounted inertial sensors. *Med. Eng. Phys.* **35**, 690-695, (2013).
- (17) Nokes, L., Fairclough, J. A., Mintowt-Czyz, W. J., Mackie, I. & Williams, J. Vibration analysis of human tibia: the effect of soft tissue on the output from skin-mounted accelerometers. *Journal of biomedical engineering* **6**, 223-226, (1984).
- (18) Ziegert, J. C. & Lewis, J. L. The Effect of Soft Tissue on Measurements of Vibrational Bone Motion by Skin-Mounted Accelerometers. *Journal of Biomechanical Engineering* **101**, 218-220, (1979).
- (19) Stefanczyk, J. M., Brydges, E. A., Burkhart, T. A., Altenhof, W. & Andrews, D. M. Surface Accelerometer Fixation Method Affects Leg Soft Tissue Motion Following Heel Impacts. *International Journal of Kinesiology and Sports Science* **1**, 1-8, (2013).
- (20) Lafortune, M. A., Henning, E. & Valiant, G. A. Tibial shock measured with bone and skin mounted transducers. *J Biomech* **28**, 989-993, (1995).
- (21) Rubin, C. *et al.* Transmissibility of 15-hertz to 35-hertz vibrations to the human hip and lumbar spine: determining the physiologic feasibility of delivering low-level anabolic mechanical stimuli to skeletal regions at greatest risk of fracture because of osteoporosis. *Spine* **28**, 2621-2627, (2003).
- (22) Baig, H. A., Guarino, B. B., Lipschutz, D. & Winkelstein, B. A. Whole body vibration induces forepaw and hind paw behavioral sensitivity in the rat. *Journal of Orthopaedic Research* **11**, 1739-1744, (2013).
- (23) Christiansen, B. A., Bayly, P. V. & Silva, M. J. Constrained tibial vibration in mice: A method for studying the effects of vibrational loading of bone. *J. Biomech. Eng.-Trans. ASME* **130**, 044502, (2008).
- (24) Rubin, C. *et al.* Quantity and quality of trabecular bone in the femur are enhanced by a strongly anabolic, noninvasive mechanical intervention. *J Bone Miner Res* **17**, 349-357, (2002).

- (25) Rubin, C. T., Sommerfeldt, D. W., Judex, S. & Qin, Y.-X. Inhibition of osteopenia by low magnitude, high-frequency mechanical stimuli. *Drug Discovery Today* **6**, 848-858, (2001).
- (26) Edelstein, A., Amodaj, N., Hoover, K., Vale, R. & Stuurman, N. *Computer Control of Microscopes Using  $\mu$ Manager*. (John Wiley & Sons, Inc., 2010).
- (27) Griffin, M. J. *Handbook of human vibration*. (Academic Press, 1990).
- (28) Schneider, C. A., Rasband, W. S. & Eliceiri, K. W. NIH Image to ImageJ: 25 years of image analysis. *Nature methods* **9**, 671-675, (2012).
- (29) Nemani, A. & Yokota, H. in *Bioengineering Conference (NEBEC), 2011 IEEE 37th Annual Northeast*. 1-2.
- (30) Kim, Y. H., Byun, C. H. & Oh, T. Y. in *Experimental Mechanics in Nano and Biotechnology, Pts 1 and 2* Vol. 326-328 *Key Engineering Materials* (eds S. B. Lee & Y. J. Kim) 851-854 (Trans Tech Publications Ltd, 2006).
- (31) Judex, S., Lei, X., Han, D. & Rubin, C. Low-magnitude mechanical signals that stimulate bone formation in the ovariectomized rat are dependent on the applied frequency but not on the strain magnitude. *J. Biomech.* **40**, 1333-1339, (2007).
- (32) LA, G.-T., MJ, G.-B., M, D. & JM., G.-A. Influence of the frequency of the external mechanical stimulus on bone healing: A computational study. *Medical Engineering and Physics* **32**, 363-371, (2010).
- (33) Wehrle, E. *et al.* Distinct frequency dependent effects of whole-body vibration on non-fractured bone and fracture healing in mice. *Journal of Orthopaedic Research* **32**, 1006-1013, (2014).
- (34) Zhao, L., Dodge, T., Nemani, A. & Yokota, H. Resonance in the mouse tibia as a predictor of frequencies and locations of loading-induced bone formation. *Biomech Model Mechanobiol* **13**, 141-151, (2013).
- (35) Matsumoto, Y. & Griffin, M. J. Dynamic Response of the Standing Human Body Exposed to Vertical Vibration: Influence of Posture and Vibration Magnitude. *Journal of Sound and Vibration* **212**, 85-107, (1998).

## Chapter 4

### 4 Conclusions and Future Directions

#### 4.1 Summary

Whole-body vibration (WBV) has shown promising potential in becoming an alternative osteoporosis intervention to drug-only therapy<sup>1-3</sup>. However, more research is needed to determine what vibration protocol is the safest and the most effective for a given demography. Small-animal models, such as mice, play an important part in answering these questions, since they are readily available, cost-effective, and have similar skeletal response as humans. However, one of the difficulties associated with mice is the fact that their small size also limits the size of instrumentation that can be attached on the animal without becoming a significant burden on the animal. Thus, in WBV study of mice, this factor attributes to the challenge of *in vivo* vibration characterization. As such, studies have only reported the effects of whole-body vibration in small-animal models, but not how much of it is actually transmitted into the skeletal system. A few studies have attempted to quantify transmission of vibration in mice, but none of them was able to characterize vibration *in vivo* and in an unsedated condition (full weight bearing on the limbs). For example, Christian *et al.*<sup>4</sup> was only able to report the tibial bone vibration characteristics and also only in an *ex vivo* environment (femur dissected). Another study measured vibration transmission at the skin level in an anesthetized rat using an inertia-based method.<sup>5</sup> Therefore, the goal of this thesis was to develop a method to characterize transmission of vibration in mice during whole-body vibration. Most importantly, the characterization is done on the skeletal level because at the skin level the vibration is attenuated by soft tissues that surround the bone, as shown from studies in human.<sup>6-9</sup> It can be expected that soft tissue would also have an influence on vibration transmission in mice. In addition, the mice would be kept unsedated, so that their limbs would be subjected to normal weight bearing.

We approached this vibration characterization problem using an imaging based method, as this does not require attachment of any sensors or instruments onto the animal. We

chose x-ray imaging as the main imaging modality since it allows us to see the animal on the skeletal level. Thus, a simple digital x-ray imaging system was constructed using commercially available components, and integrated with a whole-body vibration platform, as described in detail in Chapter 2. The system employed an indirect x-ray imaging method, *i.e.*, x-ray photon is converted to visible photon via a scintillating screen before being imaged by a CCD camera. We would prefer to quantify motion by modeling the change in pixel intensity of the bone, but one of the problems is that bone is difficult to model mathematically on an image because its pixel intensity does not stay consistent and its orientation could be different in each image. We, therefore, proposed the use of fiducial markers to track motion. Specifically, 280  $\mu\text{m}$  diameter tungsten carbide beads were implanted in the animal in the femoral and tibial bone. The pixel intensity profile of the bead on the x-ray image is a 2-D Gaussian surface, which is mathematically simple to quantify. There are three ways of tracking the marker during vibration, long-exposure imaging, stroboscopic imaging, and high-speed imaging. Given the technical limitation of the x-ray tube and the CCD camera, only long-exposure imaging was viable for our setup. Consequently, the markers exhibit motion blurring on the x-ray image. However, we found an empirical relationship between vibration amplitude and the intensity profile of the bead. Specifically, we related the full-width-at-half-maximum (FWHM), which is derived from intensity profile of the marker, to the vibration amplitude. By using this method we were able to measure the vibration amplitude in the tibial bone, or femoral bone, of a mouse during whole-body vibration. Lastly, since the mouse is unanesthetized during the experiment, it was necessary to restrain the animal such that it would remain still. We developed a simple mouse cage that was just big enough to contain the animal. It does not physically restrain the animal in any ways, which may affect vibration transmission. The restrainer also functioned as a reference cage, from which the input vibration was measured, which was achieved by gluing fiducial markers on the side of the restrainer.

The imaging techniques and processing described in Chapter 2 were utilized in Chapter 3 to characterize transmission of vertical vibration in mice. A total of six C57BL/6 mice were used in the experiment. Fiducial markers, following sterilization, were implanted in each mouse in the tibial bone and femoral bone, and the mice were given one month of

recovery. In the literature, it has been shown that low-magnitude ( $< 1\text{ g}$ ) and high-frequency vibration (10 – 100 Hz) were capable of inducing bone formation in animals and human.<sup>2,10-12</sup> Thus, we were interested in characterizing transmission of vibration in the range of 15 – 40 Hz and 0.09 – 0.85 g. Resonance was observed in the femur at 25 Hz, which was within range of prediction of finite element model and *ex vivo* experimentation.<sup>13,14</sup> The behavior of the tibial bone in that vibration frequency range was also consistent with the *ex vivo* result from Christiansen *et al.*<sup>4</sup> We also explored the relationship between the posture, which we defined as the angle between tibial bone and femoral bone of the animal, and transmissibility (*in vivo* vibration amplitude to reference vibration amplitude). In human whole-body vibration, the transmissibility is affected by the standing posture.<sup>15,16</sup> Likewise, in mice, we found the correlation between the transmissibility and posture to be negative. In other word, when the animal is in a crouching position (*i.e.* small tibial to femur angle), there is more vibration being transmitted to its body, and vice versa. Therefore, we have successfully characterized the transmission of vibration in mice using a non-invasive image-based method. These results may help researchers working with mice in whole-body vibration studies to estimate how much vibration is transmitted to the bone at a given vibration frequency, and thus enable them to quantify the effects of whole-body vibration as well as amount of vibration that is received at a particular region.

## 4.2 Limitations and future directions

There are several limitations with our technique. First, the imaging system limits the smallest vibration amplitude that could be imaged. The effective pixel resolution with our current setup is about 33  $\mu\text{m}/\text{pixel}$ , which is sufficient to detect vibration amplitude of at least 80  $\mu\text{m}$ . It is important to note that the vibration amplitude is inversely proportional to square of vibration frequency, if the peak-acceleration is kept constant.<sup>17</sup> Thus, the higher the vibration frequency, the smaller the vibration amplitude would be. This is the reason why we were only able to characterize transmission of vibration from 15–40 Hz. For instance, for vibration frequency of 70 Hz at 0.43 g, the corresponding vibration is only 22  $\mu\text{m}$ , which is too small for our imaging system to differentiate. If we wish to characterize vibration at higher frequency, we would need to increase the resolution of

the CCD camera or change the optics of the CCD camera. However, these changes would decrease the overall field of view of the image, which reduces number of fiducial markers that could be imaged. One possible solution is to use smaller fiducial markers ( $< 200 \mu\text{m}$ ), which may be more sensitive to smaller vibration amplitude than bigger fiducial marker; however, small markers will also provide lower radiographic contrast. It is also worthy to note that our imaging time (630 ms) is much longer than any of the vibration periods used in this study (e.g. 67 ms, 50 ms, 40 ms, 33 ms, 29 ms, 25 ms). This enables us to see the motion blur. Consequently, the temporal information of the bead is lost, *i.e.*, vibration frequency. Thus, this technique is not able to determine the vibration frequency *in vivo*; this should not be a problem in our studies, as we apply a sinusoidal waveform at a known vibration frequency. A previous study has shown that a phase difference in frequency may exist *in vivo*.<sup>4</sup> We expect the same thing would occur in mice, but just how much of difference from the input vibration frequency remains a research question yet to be answered.

Second, while it was relatively easy process to implant the bead, the location of implantation is rather selective. This is due to the anatomy of the animal, making some regions of the bone easier to access than others, without being more invasive. Therefore, the implantation location is very limited. This constraint limits our ability to study vibration characteristics in different regions of the same bone. Research questions such as, “Does local bone formation contribute to increased vibration transmission at that region?” cannot be answered with our technique. The use of bone cement could resolve this problem. Specifically, instead of implanting the bead into the bone, one could glue the bead onto the bone. This procedure would allow us to put the bead in any location without worrying about the invasiveness of the procedure. However, in our experiment, we did not explore this possibility.

Lastly, the mouse restrainer is not perfect. The mice were able to turn their bodies within the restrainer, which prolonged imaging time. The restrainer had to be re-orientated each time in order to obtain the correct field of view when the animal changes its position in the restrainer. In addition, the restrainer was not able to eliminate random movements of the animal, such as grooming. Images contain blur caused by random motion were



rejected from our data analysis. Finally, the x-ray tube also has its technical limitation in terms of number of images that could be taken within a time span. Recall that the x-ray energy was 80 kV<sub>p</sub> at 200 mA. The combination of high energy with exposure of 630 ms and multiple successive image acquisitions would cause to the x-ray tube to overheat rapidly. Therefore, for each image, one minute cool down time was required. This further prolongs the imaging time.

Looking ahead, this technique of quantifying vibration amplitude using motion blur could be used to determine how tissue-level vibration and skeletal-level vibration compares in mice. Since the bead is small, it could be attached directly onto the skin of the animal without introducing significant weight burden on the limb. The vibration amplitude could be then determined, based the motion blur of the bead on an x-ray image. This technique can also be extended to other small animals such as rabbits and rats, and the surgical procedure becomes easier as the size of the animal increases. As mentioned previously from Chapter 2, this quantification technique has the potential to be used in human experiments as well. Specifically, in subjects who have implanted fiducial markers for the purpose of knee or hip implant position localization (*i.e.* radiostereometric analysis). Thus, no additional surgery is required for bone-mounted accelerometers.

### 4.3 Conclusion

This thesis has introduced an imaging-based method of quantifying vertical vibration transmission, specifically in a small animal such as mice. The construction of a simple digital x-ray imaging system, which incorporated a whole-body vibration platform, was discussed in detail. Also, the theoretical background associated with inferring vibration amplitude from motion blur was discussed. We validated our technique by characterizing transmission of vertical vibration in six C57BL/6 mice in the 15 – 40Hz range. We observed a resonance in the femoral bone at 25 Hz, and a reduction of transmission in the tibial bone at 30 Hz. We also observed a negative correlation between the transmissibility and animal posture. The imaging system could be improved with higher pixel resolution, which would enable characterization in the higher frequency range (> 40 Hz). Moreover, this technique can be adapted to other small animal models.

## References

- (1) Rubin, C., Judex, S. & Qin, Y.-X. Low-level mechanical signals and their potential as a non-pharmacological intervention for osteoporosis. *Age Ageing* **35 Suppl 2**, ii32-36, (2006).
- (2) Rubin, C., Turner, A. S., Bain, S., Mallinckrodt, C. & McLeod, K. Anabolism. Low mechanical signals strengthen long bones. *Nature* **412**, 603-604, (2001).
- (3) Banu, J., Varela, E. & Fernandes, G. Alternative therapies for the prevention and treatment of osteoporosis. *Nutrition reviews* **70**, 22-40, (2012).
- (4) Christiansen, B. A., Bayly, P. V. & Silva, M. J. Constrained tibial vibration in mice: A method for studying the effects of vibrational loading of bone. *J. Biomech. Eng.-Trans. ASME* **130**, 044502, (2008).
- (5) Baig, H. A., Guarino, B. B., Lipschutz, D. & Winkelstein, B. A. Whole body vibration induces forepaw and hind paw behavioral sensitivity in the rat. *Journal of Orthopaedic Research* **11**, 1739-1744, (2013).
- (6) Kim, W., Voloshin, A. S., Johnson, S. H. & Simkin, A. Measurement of the Impulsive Bone Motion by Skin-Mounted Accelerometers. *J. Biomech. Eng.-Trans. ASME* **115**, 47-52, (1993).
- (7) Nokes, L., Fairclough, J. A., Mintowt-Czyz, W. J., Mackie, I. & Williams, J. Vibration analysis of human tibia: the effect of soft tissue on the output from skin-mounted accelerometers. *Journal of biomedical engineering* **6**, 223-226, (1984).
- (8) Stefanczyk, J. M., Brydges, E. A., Burkhart, T. A., Altenhof, W. & Andrews, D. M. Surface Accelerometer Fixation Method Affects Leg Soft Tissue Motion Following Heel Impacts. *International Journal of Kinesiology and Sports Science* **1**, 1-8, (2013).
- (9) Ziegert, J. C. & Lewis, J. L. The Effect of Soft Tissue on Measurements of Vibrational Bone Motion by Skin-Mounted Accelerometers. *Journal of Biomechanical Engineering* **101**, 218-220, (1979).
- (10) Chen, B., Li, Y., Xie, D. & Yang, X. Low-magnitude high-frequency loading via whole body vibration enhances bone-implant osseointegration in ovariectomized rats. *Journal of Orthopaedic Research* **30**, 733-739, (2012).
- (11) Gilsanz, V. *et al.* Low-level, high-frequency mechanical signals enhance musculoskeletal development of young women with low BMD. *J Bone Miner Res* **21**, 1464-1474, (2006).
- (12) Verschueren, S. M. P. *et al.* Effect of 6-month whole body vibration training on hip density, muscle strength, and postural control in postmenopausal women: A randomized controlled pilot study. *J Bone Miner Res* **19**, 352-359, (2004).

- (13) Kim, Y. H., Byun, C. H. & Oh, T. Y. in *Experimental Mechanics in Nano and Biotechnology, Pts 1 and 2* Vol. 326-328 *Key Engineering Materials* (eds S. B. Lee & Y. J. Kim) 851-854 (Trans Tech Publications Ltd, 2006).
- (14) Nemani, A. & Yokota, H. in *Bioengineering Conference (NEBEC), 2011 IEEE 37th Annual Northeast*. 1-2.
- (15) Matsumoto, Y. & Griffin, M. J. Dynamic Response of the Standing Human Body Exposed to Vertical Vibration: Influence of Posture and Vibration Magnitude. *Journal of Sound and Vibration* **212**, 85-107, (1998).
- (16) Crewther, B., Cronin, J. & Keogh, J. Gravitational forces and whole body vibration: implications for prescription of vibratory stimulation. *Phys. Ther. Sport* **5**, 37-43, (2004).
- (17) Griffin, M. J. *Handbook of human vibration*. (Academic Press, 1990).

## Appendix A: Ethics Approval

**From:** eSiriusWebServer  
**To:** Stephen Sims  
**CC:** auspc@uwo.ca  
**Date:** 11/12/2013 2:39 PM  
**Subject:** eSirius Notification - New Protocol Modification Has Been APPROVED2008-043-06::6



AUP Number: 2008-043-06  
 PI Name: Sims, Stephen M  
 AUP Title: Role of cytosolic calcium in the regulation of osteoclasts and bone resorption// Ion Transport and Signalling in Skeletal Cells: P2 Nucleotide Receptor Function in Bone

**Official Notification of AUS Approval:** A MODIFICATION to Animal Use Protocol 2008-043-06 has been approved.

The holder of this Animal Use Protocol is responsible to ensure that all associated safety components (biosafety, radiation safety, general laboratory safety) comply with institutional safety standards and have received all necessary approvals. Please consult directly with your institutional safety officers.

Submitted by: Kinchlea, Will D  
 on behalf of the Animal Use Subcommittee



electrical property as a new contrast  
 mechanism


*The University of Western Ontario*  
 Animal Use Subcommittee / University Council on Animal Care  
 Health Sciences Centre, • London, Ontario • CANADA – N6A 5C1  
 PH: 519-661-2111 ext. 86768 • FL 519-661-2028  
 Email: [auspc@uwo.ca](mailto:auspc@uwo.ca) • <http://www.uwo.ca/animal/website/>

tr.grid\_heading {background-color: steelblue; font-family: verdana, sans-serif, times; font-weight: bold; font-size: 9px; color: white; text-align: center} tr.grid\_data\_row {background-color: white; font-family: verdana, sans-serif, times; font-weight: normal; font-size: 9px; color: black} p.messageBody {font-family: verdana, sans-serif, times; font-size: 10pt; color: black; text-align: left} p.right{float: right;margin-right:

## Appendix B: Copyright Permissions

Permission for Figure 1-1.

HomeAccount InfoHelp



**Title:** Bone Remodeling in Post-menopausal Osteoporosis:  
**Author:** U.H. Lerner  
**Publication:** Journal of Dental Research  
**Publisher:** SAGE Publications  
**Date:** 07/01/2006

Copyright © 2006, International & American Associations for Dental Research

Logged In as:  
Zhengyi Hu  
Account #:  
3000820557

LOGOUT

**Gratis**

Permission is granted at no cost for sole use in a Master's Thesis and/or Doctoral Dissertation. Additional permission is also granted for the selection to be included in the printing of said scholarly work as part of UMI's "Books on Demand" program. For any further usage or publication, please contact the publisher.

BACKCLOSE WINDOW

Copyright © 2014 [Copyright Clearance Center, Inc.](#) All Rights Reserved. [Privacy statement.](#)  
Comments? We would like to hear from you. E-mail us at [customercare@copyright.com](mailto:customercare@copyright.com)

Permission for Figure 1-2.



RightsLink®

Home

Account Info

Help



WILEY

**Title:** A simple method for correlative light and scanning electron microscopy of human iliac crest bone biopsies: Qualitative observations in normal and osteoporotic subjects

**Author:** D. W. Dempster, E. Shane, W. Horbert, R. Lindsay

**Publication:** Journal of Bone and Mineral Research

**Publisher:** John Wiley and Sons

**Date:** Dec 3, 2009

Copyright © 1986 ASBMR

Logged In as:  
Zhengyi Hu  
Account #:  
3000820557

LOGOUT

### Order Completed

Thank you very much for your order.

This is a License Agreement between Zhengyi Hu ("You") and John Wiley and Sons ("John Wiley and Sons"). The license consists of your order details, the terms and conditions provided by John Wiley and Sons, and the [payment terms and conditions](#).

[Get the printable license.](#)

License Number	3453800379152
License date	Aug 21, 2014
Licensed content publisher	John Wiley and Sons
Licensed content publication	Journal of Bone and Mineral Research
Licensed content title	A simple method for correlative light and scanning electron microscopy of human iliac crest bone biopsies: Qualitative observations in normal and osteoporotic subjects
Licensed copyright line	Copyright © 1986 ASBMR
Licensed content author	D. W. Dempster, E. Shane, W. Horbert, R. Lindsay
Licensed content date	Dec 3, 2009
Start page	15
End page	21
Type of use	Dissertation/Thesis
Requestor type	University/Academic
Format	Print and electronic
Portion	Figure/table
Number of figures/tables	2
Original Wiley figure/table number(s)	Figure 5c and Figure 5d
Will you be translating?	No
Title of your thesis / dissertation	THE DEVELOPMENT OF A DIGITAL X-RAY IMAGING SYSTEM FOR THE CHARACTERIZATION OF TRANSMISSION OF WHOLE-BODY VIBRATION IN MICE
Expected completion date	Aug 2014
Expected size (number of pages)	82
Total	0.00 USD

ORDER MORE...

CLOSE WINDOW

## Curriculum Vitae

**Name:** Zhengyi Hu

**Post-secondary Education and Degrees:** Western University  
London, Ontario, Canada  
2011-2014 M.Sc. Candidate

York University  
Toronto, Ontario, Canada  
2006-2011 B.Sc.

**Honours and Awards:** Western Graduate Research Scholarship  
2011-2013

Western Three-Minute Thesis Finalist  
2012

Singapore International pre-graduate award  
2012

Michael H. Lawee Memorial Award in Science & Engineering  
2007

**Related Work Experience** Research Assistant  
Robarts Research Institute, London, ON, Canada  
2011-2014

Research Intern  
Institute for Infocomm Research (I<sup>2</sup>R), A\*STAR, Singapore  
2012

### Papers in preparation:

**Z. Hu**, I. Welch, X. Yuan, S. Pollmann, H. Nikolov, D. Holdsworth. Quantification of mouse *in vivo* whole-body vibration amplitude from motion-blur using x-ray imaging. In preparation for submission to *Physics in Medicine and Biology*.

**Z. Hu**, I. Welch, X. Yuan, J. Dixon, D. Holdsworth. Transmission of vertical whole-body vibration in mice. In preparation for submission to *Journal of Bone and Mineral Research*.

### **Poster Presentations:**

**Z. Hu, D. Holdsworth.** Transmission of whole body vibration in mice. 12<sup>th</sup> Imaging Network Ontario Conference, Toronto, Ontario, Canada (03/14)

**Z. Hu, D. Holdsworth.** In vivo quantification of whole body vibration in mice. London Health Research Day, London, Ontario, Canada (02/13)

**Z. Hu, M. F. Karim, L. C. Ong, B. Luo, and T. M. Chiam.** A Simple and Efficient Method of Millimeter-wave Image Formation using Back-projection Algorithm. Asia-Pacific Microwave Conference, Seoul, Korea (11/13)

**Z. Hu, D. Holdsworth.** In vivo quantification of whole body vibration in mice. London Imaging Discovery, London, Ontario, Canada (06/13)

**Z. Hu, D. Holdsworth.** In vivo quantification of whole body vibration in mice. London Health Research Day, London, Ontario, Canada (03/13)

**Z. Hu, D. Holdsworth.** Development of a high-resolution digital x-ray imaging system for quantifying whole-body vibration. 11<sup>th</sup> Imaging Network Ontario Conference, Toronto, Ontario, Canada (02/13)

**Z. Hu, D. Holdsworth.** Development of a high-resolution digital x-ray imaging system for quantifying whole-body vibration. Western Research Forum, London, Ontario, Canada (04/12)

### **Oral Presentations**

**Z. Hu, D. Holdsworth.** A simple in-vivo whole-body vibration quantification technique based on motion blur. Bone and Joint Conference, London, Ontario, Canada (01/14)

### **Leadership and Volunteer Activities**

2011-2014     Radio co-host, Western Worlds

2010-2011     Vice-president, Astronomy club at York University

2007-2011     Senior Observatory Staff, York University Observatory

2007-2010     Executive Member, York University Rover Team

2004-2006     Youth member, Royal Astronomical Society of Canada